Title	Calcite sealing in a fractured geothermal reservoir: Insights from combined EBSD and chemistry mapping
Author(s)	McNamara, David D.; Lister, Aaron; Prior, Dave J.
Publication Date	2016-05-10
Publication Information	McNamara, David D., Lister, Aaron, & Prior, Dave J. (2016). Calcite sealing in a fractured geothermal reservoir: Insights from combined EBSD and chemistry mapping. Journal of Volcanology and Geothermal Research, 323, 38-52. doi: http://dx.doi.org/10.1016/j.jvolgeores.2016.04.042
Publisher	Elsevier
Link to publisher's version	https://doi.org/10.1016/j.jvolgeores.2016.04.042
Item record	http://hdl.handle.net/10379/6726
DOI	http://dx.doi.org/10.1016/j.jvolgeores.2016.04.042

*Revision, changes accepted
Click here to view linked References

Calcite sealing in a fractured geothermal reservoir: Insights from combined EBSD and chemistry mapping

David D. McNamara, GNS Science, Lower Hutt, New Zealand
Aaron Lister, Department of Geology, University of Otago, Dunedin, New Zealand
Dave J. Prior, GNS Science, Department of Geology, University of Otago, Dunedin, New Zealand

Corresponding author: D. D. McNamara, 1 Fairway Drive, GNS Science, Lower Hutt, New Zealand, 5040. (d.mcnamara@gns.cri.nz)

Abstract

Fractures play an important role as fluid flow pathways in geothermal resources hosted in indurated greywacke basement of the Taupo Volcanic Zone, New Zealand, including the Kawerau Geothermal Field. Over time, the permeability of such geothermal reservoirs can be degraded by fracture sealing as minerals deposit out of transported geothermal fluids. Calcite is one such fracture sealing mineral. This study, for the first time, utilises combined data from electron backscatter diffraction and chemical mapping to characterise calcite vein fill morphologies, and gain insight into the mechanisms of calcite fracture sealing in the Kawerau Geothermal Field. Two calcite sealing mechanisms are identified 1) asymmetrical syntaxial growth of calcite, inferred by the presence of single, twinned, calcite crystals spanning the entire fracture width, and 2) 3D, interlocking growth of bladed vein calcite into free space as determined from chemical and crystallographic orientation mapping. This study also identifies other potential uses of combined EBSD and chemical mapping to understand geothermal field evolution including, potentially informing on levels of fluid supersaturation from the study of calcite lattice distortion, and providing information on a reservoir's history of stress, strain, and deformation through investigation of calcite crystal deformation and twinning patterns.

Introduction

Development of natural and enhanced geothermal resources, hosted in crystalline, volcanic, plutonic or, metamorphic basement reservoirs, has increased over recent years [Wood et al., 2001; Asanuma et al., 2005; Sausse et al., 2006; Blackwell et al., 2007; Bertani, 2012]. In these reservoir rocks, permeability is dominated by faults and fractures, with small contributions made by primary permeability [Brace, 1980; Davatzes and Hickman, 2010a; Dezayes et al., 2010]. As such, the study of how these structures are generated, their properties (e.g. orientation, spatial distribution, aperture, orientation with respect to the stress field), how they become filled with precipitated minerals, and their crack-seal cycle history is vital to understanding the evolution of geothermal systems and to their successful development. Progressive fracture sealing (i.e. vein formation) is known to create barriers and baffles to fluid flow in a geothermal reservoir, decreasing overall permeability and limiting the reservoir's effectiveness as a resource [Batzle and Simmons, 1976; Dobson et al., 2003; Genter et al., 2010]. Study of this sealing process is vital to discerning the evolution and sustainability of fractured geothermal systems.

Fracture sealing creates veins which can be used to determine aspects of the geological history of the host rock. The mineralogy, geochemistry, microstructure, and fluid inclusion analysis of vein minerals provides information on pressure and temperature conditions of the reservoir rock, stress and strain that was occurring at or after the time they were precipitated, and on the composition and origin of related fluids. Vein formation (fracture sealing) is achieved by the precipitation of minerals from the circulating fluids, or from water-rock interactions, within geothermal systems, and can occur as a single precipitation event or as multiple crack-sealing events [Ramsay, 1980]. Evidence for multiple sealing events comes from observation of multiple mineral phases, or sequential depositions of the same mineral phase in a vein. The classification of veins can be broken into i) syntaxial, ii) stretching, iii) antitaxial, and iv) pressure shadows/fringes (Figure 1) [Bons et al., 2012]. Syntaxial veins form where mineral growth occurs from one of or both fracture faces toward the centre, with crystals often becoming elongate in the growth direction. Syntaxial vein minerals often show lattice preferred orientations that strengthen with distance from the fracture wall as growth competition eliminates those crystals not oriented to the fast growth direction [Cox and Etheridge, 1983; Bons, 2001; Nüchter and Stöckhert, 2007; Okamoto and Sekine, 2011]. Stretching veins grow in a similar way to syntaxial veins [Durney and Ramsay, 1973] but the crack surface cuts through previously precipitated vein crystals (localised stretching veins) or wall rock (delocalised stretching veins) as opposed to the mineral growth surface. Due to their similarity a continuum exists between syntaxial and stretching veins. Localised stretching veins can seal a crack from both crack surfaces (bitaxial) or from one surface (unitaxial) [Hilgers et al., 2000]. Antitaxial veins grow from a median suture in a fracture toward the fracture walls and usually contain fibrous crystals. They are defined by the presence of a median line/zone across which two-fold rotational symmetry is often observed in the fibre pattern. It is thought that antitaxial veins grow by crack-seal mechanisms, or that growth occurs on the closed interface between vein and wall rock. Antitaxial vein growth is also possible as a result of crystal growth, in a diffusional mass transfer (DMT) system, exerting outward force that pushes the wall rock apart [Wiltschko and Morse, 2001]. Pressure shadows/fringes are a unique type of vein that forms in pressure shadows occurring next to a rigid object in a deforming material.

Determination of mineral sealing processes from microstructural and chemical data is made difficult due to the processes being highly sensitive to a wide range of factors; degree of fluid supersaturation, anisotropic growth kinetics (mineral growth), rates of local deformation, and rates of fluid transport [Hilgers et al., 2004]. Calcite is a common mineral in many geological systems and geothermal reservoirs are no exception. Calcite is usually found in geothermal systems with temperatures of ~140-300°C and where fluids have high concentrations of dissolved CO_2 [Simmons and Christenson, 1994; Browne, 1978] occurring both as a replacement of parent rock mineral phases, or as cement or vein fill. Hydrothermal calcite veins have been reported in geothermal systems in North America [Batzle and Simmons, 1976; Dobson et al., 2003], the granite, enhanced geothermal reservoir of Soultz-sous-Forêts [Hébert et al., 2011], and in several geothermal fields located in the Taupo Volcanic Zone (TVZ), New Zealand [Krupp and Seward, 1987; Hedenquist, 1990; Wood et al., 2001]. The precipitation of hydrothermal calcite is controlled dominantly by the movement of CO_2 in the reservoir as governed by boiling, dilution, and condensation, and to a lesser extent by pH, temperature, and the aqueous calcium ion activity [Fournier, 1985; Simmons and Christenson, 1994]. As a result, calcite is a highly reactive mineral in a geothermal system such that varying temperature profiles along fluid flow pathways create zones where it can be dissolved and zones where it can be precipitated. Colder, circulating fluids often result in calcite dissolution, which, due to calcite's retrograde solubility (decreases with increasing temperature), is then precipitated back out elsewhere as the circulating fluid temperature increases [André et al., 2006]. Platy calcite (also known as bladed calcite) is commonly found in veins and voids in geothermal reservoir rocks and is the result of precipitation from boiling fluids through the exsolution of CO_2. Observations of bladed calcite in geothermal wells are made by Tulloch [1982] who noted that the platy crystals grow outward from the walls in a direction perpendicular to the **c**-axis at a rate of ~0.1mm/day.

The common occurrence of calcite as a fracture sealing mineral in geothermal fields makes it an ideal case study for examining hydrothermal fracture sealing. This work examines calcite-filled fractures from a sample of greywacke reservoir rock from the Kawerau Geothermal Field using, for the first time, combined chemical mapping techniques (cathodoluminescence (CL) and electron diffraction x-ray (EDX)), and electron backscatter diffraction (EBSD). Similar combinative studies attempting to infer the connection between microstructure and chemistry in veining are rare [Bons et al., 2012 and references therein] and many are more focused on detailed chemical and isotopic analyses [Barker et al., 2006; Barker et al., 2009]. This paper aims to utilise these combined techniques to determine how hydrothermal calcite growth occurs in geothermal fractures, explore what the microstructure can tell us about the crack-seal evolution of the greywacke basement of the Kawerau Geothermal Field, and the implications this may have for reservoir permeability.

Geological Setting

The Kawerau Geothermal Field is the most northern, active, high temperature (>300°C), geothermal field in the TVZ (Figure 2). The TVZ represents the active part of the Central Volcanic Region (CVR), an extensional intra-arc basin formed as a result of subduction of the Pacific Plate beneath the North Island of New Zealand [Wilson et al., 1995; Cole and Spinks, 2009; Begg and Mouslopoulou, 2010; Rowland and Simmons, 2012]. The TVZ is segmented structurally, by offsets in its rift axis [Rowland and Sibson 2001], and magmatically, such that the central TVZ is dominated by rhyolitic volcanism, while the north and south portions experience andesitic-dacitic volcanism [Rowland and Simmons, 2012; Wilson et al, 1995]. Rifting commenced 1-2 Ma and continues to the present day with extension rates decreasing from ~15 mm/yr at the coast of the Bay of Plenty to ~3 mm/yr near the rift termination (south of Lake Taupo) [Villamor and Berryman, 2001; Wallace at al., 2004; Begg and Mouslopoulou, 2010; Chambefort et al., 2014]. Extension in the TVZ is accommodated by the Taupo Rift, a series of dominantly NE-SW striking, normal faults with a vertical maximum principal stress (σ_1/S_v), a NW-SE extension/minimum horizontal stress direction (σ_3/S_{hmin}), and a NE-SW maximum horizontal stress direction (σ_2/S_{Hmax}) [Nicol et al., 2006, Hurst et al., 2008, McLean and McNamara et al., 2011; Wallis et al., 2012; Townend et al., 2012; McNamara et al., 2015].

The Whakatane Graben, which subsides at rates >0.8 m/ky [Nairn and Beanland, 1989], is situated where the normal faulting of the TVZ intersects with the dominantly strike slip faults of the North Island Dextral Shear Belt [Begg and Mouslopoulou, 2010; Villamor et al., 2011]. The Kawerau geothermal reservoir is located within the Whakatane Graben where rhyolite dominated volcanism of the central TVZ transitions into the andesite-dacite volcanism of the north TVZ segment [Wilson et al., 1995; Nairn, 2002]. The geothermal resource is hosted in Mesozoic greywacke basement composed of medium-grained, andesite-dacite sourced sandstones with minor argillite and chert. The hosting basement terrane for the Kawerau geothermal resource has been debated to be either the Torlesse [Wood et al., 2001] or the Waipapa [Adams et al., 2009]. It is thought that the transition between basement greywacke terranes in the TVZ occurs under or near the Kawerau Geothermal Field [Adams et al., 2009; Leonard et al., 2010; Milicich et al., 2013]. The geothermal reservoir is overlain by ~1km of Quaternary volcano-sedimentary deposits. Fluid flow within the greywacke basement of the Kawerau system is dominated and controlled by a series of faults and fractures as evident from NE-SW trending lineaments of hydrothermal features [Christenson, 1987], the spatial relation of structures imaged with borehole televiewers to zones of permeability (as measured by pressure, temperature, and fluid velocity logs) [Wallis et al., 2012], and the low permeability of the intact greywacke rock itself [Christenson, 1987; McNamara et al., 2014]. Geothermal well performance indicates that while the north of the Kawerau Geothermal Field hosts permeability controlled by active structures, similar structures present in the south of the field, are likely inactive and sealed by hydrothermal mineral deposition, thus restricting permeability in this area [Christenson, 1997; Bignall and Milicich, 2012; Milicich et al., 2013].

Sample Petrography

A sample of un-oriented, greywacke basement drill-core from well KA30 (comprising the interval 1098-1100 mRF), in the southern area of Kawerau Geothermal Field, was utilised for this work. A piece of the drill-core, displaying several intersecting veins, was thin-sectioned (Figure 3). The greywacke is a clast supported, matrix poor, medium to coarse grained greywacke sandstone (0.25 – 1.5 mm) consisting of subangular - subrounded detrital quartz (10%), plagioclase and biotite/phlogopite (30%), and lithic fragments (50%). Lithic fragments include porphyritic lavas, rare plutonic fragments, and siltstone and sandstone fragments. The matrix is composed of indurated clay/silt. This greywacke is moderately altered with a hydrothermal assemblage of chlorite, leucoxene (a granular alteration product of titanium-rich minerals), hydrothermal clays, and minor amounts of wairakite (zeolite; $Ca_8(Al_{16}Si_{32}O_{96})*16H_2O$), epidote and disseminated pyrite.

The greywacke sample used in this study contains a complex set of cross cutting, mineralised fractures filled with calcite, wairakite, and small amounts of pyrite (Figure 3). The youngest fracture set tends to be wider (~1 - 1.5 mm) than the older fractures they cross-cut and contain calcite as their only mineral fill. Calcite in these veins are either elongate (1 - 1.5 mm) in appearance (a texture known as bladed calcite), particularly in the wider veins, or have a blocky form. Smaller calcite crystal sizes, with irregular shape are observed nearer the fracture walls. Older fracture generations are filled with mixtures of calcite and wairakite noted to be in textural equilibrium [Christenson, 1987]. Some of these vein textures show wairakite at fracture edges with a central calcite fill (Figure 3). The fracture fill sequences documented here are similar to those described by Absar and Blattner [1985], though we note the lack of prehnite in our study sample.

Fracturing in the Kawerau Geothermal Field reservoir is thought to be hydraulic in origin. This is supported by observed vein mineral assemblages which follow models for mineralisation in hydraulic-fracturing [Phillips, 1972; Hedenquist and Henley, 1985] in rock with high tensile strength and low intrinsic permeability, both of which are true of the greywacke basement at Kawerau [McNamara et al., 2014]. Additionally, veins are often noted to contain wall-rock fragments, providing evidence of the explosive nature of the fracturing events [Christenson, 1987]. The greywacke wall rock proximal to all fractures in the studied sample shows damage (shattered quartz, feldspar, and lithic grains, and narrow, micro-fractured, damage zones around the main fracture structures) and supports interpretation of these fractures forming during an explosive, hydrofracturing process [Christenson, 1987]. This effect is more pronounced around the older, wairakite/calcite filled fractures, than around the younger, bladed calcite filled fractures. The younger fracture generation examined in this study cross-cuts older fractures at a high angle and also cuts across larger quartz and lithic grains of the greywacke rock. Where shear markers can be identified either side of these younger fractures, small lateral offsets can be observed. The most obvious lateral offset noted is where a younger generation fracture offsets an older wairakite/calcite filled fracture by ~ 0.25 mm (Figure 3c), indicating a shear component to the younger fracture.

Fluid inclusion homogenisation temperatures, freezing point depression data, and the presence of liquid and vapour rich fluid inclusions, indicate that Kawerau basement vein calcite deposited from boiling fluids [Christenson, 1987]. The implication of a boiling parent fluid is that the confining pressure in the fracture was likely less than the hydrostatic pressure at depth. However the modal homogenisation temperatures noted by Christenson [1987] lie above the boiling point curve for water, indicating that fracture channels were also, at times, overpressured (above local hydrostatic). It is thought that this over pressurisation is a prerequisite for initiating the hydraulic fracturing in the Kawerau Geothermal Field in the first place. A combination of overpressured fluid in the fractures, and volcanic processes associated with Putauaki are thought to be responsible for the hydro-fracturing [Hedenquist and Henley, 1985; Phillips, 1972; Christenson, 1987]. Hydrofracturing, which resulted in a sudden pressure drop, is responsible for the instantaneous flashing, and rapid supersaturation of calcite in the boiling fracture fluid, which resulted in rapid precipitation of calcite on the fracture walls, often with bladed crystal morphology [Christenson, 1987]. Bladed calcite in veins at Kawerau Geothermal Field are thought to have undergone rapid growth due to observed pitted surfaces under SEM [Christenson, 1987], and observations of rapid growth of bladed calcite (~0.1 mm/day) in flowing wells at Kawerau [Tulloch, 1982].

Temperature conditions of calcite formation in veins at Kawerau Geothermal Field have been determined from fluid inclusion and stable isotope studies [Christenson, 1987; Absar, 1988]. Temperatures for the deposition of the calcite from fluid inclusion measurements have not been made on the vein samples investigated in this paper but have been reported from bladed calcite veins in nearby wells at similar depths [Christenson, 1987]. Fluid temperatures during bladed calcite precipitation are tentatively placed at ~270-305 °C. Isotope data (δO^{18}) from this calcite precipitation event indicates precipitation from meteroric fluids with a magmatic component [Absar, 1988]. The formation depth of the youngest vein generation (bladed calcite) in the investigated sample can be assumed to be ~1100 m, assuming that the bladed calcite precipitation event likely represents, at its oldest, the initiation of the modern geothermal system in Kawerau (~16000 yrs), and little erosion of cover material has occurred [Milicich et al., 2013]. This postdates the deposition of nearly all the volcanosedimentary units that overlie the greywacke basement in this area [Milicich, 2014]. Assuming a vein formation depth of 1100 m, fluid temperatures of ~270-305 °C, water density values of 1531-1846 kg/m^3, and the fact that bladed calcite precipitated from fluid under confining pressures lower than the hydrostatic pressure, an estimation of vein formation pressure is ~16-20 MPa. Attempting to determine the vein formation conditions for the older wairakite-calcite vein is more difficult. Wairakite, commonly found in hydrofractures in geothermal fields, is known to form when measured temperatures are in excess of 160°C at Kawerau, and the later calcite in this vein, likely precipitated at temperatures similar to those of the younger vein (>~270°C) [Christenson, 1987]. Isotopic studies (δO^{18}) of wairakite-prehnite veins [Absar, 1988] suggest higher fluid temperatures of 280-300 °C and that this vein fill represents an earlier deposition event from meteoric fluids that predates the deposition of calcite. The timing of this older veining event remains equivocal and the depth of its formation, and thus pressure conditions, are undetermined.

Methodology

Sample Preparation

A 30μm thick thin section (Figure 3b) was mechanically and chemically polished using diamond pastes down to 1μm followed by colloidal silica. This process minimised negative effects of surface damage and topography on EBSD mineral indexing [Prior et al., 1996]. The edges of the prepared specimen were painted with carbon and the sample surface was carbon coated (~10nm thick) to prevent charging in the SEM.

Electron Backscatter Diffraction (EBSD)

EBSD is a technique capable of rapid acquisition of large crystallographic orientation datasets of a rock's mineral phases [Prior et al., 1999]. EBSD carried out in this work was performed using a Zeiss Sigma variable pressure field emission gun SEM fitted with an Oxford Instruments Nordlys F EBSD camera and an XMax 20 silicon drift EDX detector, located at the Otago Centre for Electron Microscopy (OCEM) at the University of Otago, Dunedin. To collect EBSD patterns, the thin section was tilted 70° to the incoming electron beam allowing for a diffraction pattern to be generated on a phosphor screen. EBSD was carried out using an acceleration voltage of 30 kV, beam current of ~90nA, and a working distance of ~20 mm. Both EBSD and EDX data were collected using Oxford instruments AZTec software which undertook initial processing for both techniques. The mapped EBSD data was processed with HKL Channel5 software using methods comparable to Bestmann and Prior [2003].

Energy Dispersive X-Ray Spectroscopy (EDX) and Cathodoluminescence (CL)

EDX data were collected using Oxford Instruments AZTEC software with a XMAX20 silicon drift detector. Full spectrum EDX data were collected on a grid using an accelerating voltage of 15 to 20 kV and ~ 1-10 nA of beam current. Spectra (including map data) were processed using the TruMap and QCAL procedures within the AZTEC software. Map data presented here show counts within $K\alpha$ energy windows corrected for peak overlaps and background counts.

CL images were taken using a Technosyn cold cathode stage mounted on an Olympus BX41 microscope with a trinoc head fitted with a digital camera. The CL apparatus was operated under vacuum (0.05-0.08 Torr / 17-20 V) at an accelerating voltage of 15-20 kV and a beam current of 550-600 μA.

Results

Cathodoluminescence (CL)

Figure 4 shows CL images of the fractures in the sample: colours vary from fracture to fracture. The youngest generation of fracturing shows bright, yellow/orange coloured calcite (Figure 4b) while the older fractures, cross-cut by the younger fractures, contain wairakite (dull, purple/blue CL colours) and calcite (dull, darker orange/red CL colours) (Figure 4c). Individual calcite crystals in all fracture generations show variation of the orange/red CL colours, implying they are chemically zoned. Yellow cathodoluminesence in calcite is linked to higher Mn content, whereas red CL response is proportional to Fe content [Long and Agrell, 1965]. Visa versa, the more red the CL colour the higher the Fe content and lower the Mn content.

Zonation in CL is more pronounced in calcite crystals sealing the younger generation of fractures (Figure 4e). These calcite crystals show complicated zonation patterns. In some elongate calcite crystals, concentric zonation stretches along the crystal long axes in bands (Figure 4e, 11). This concentric banding varies in width along the crystal axes; thinner along the long edges of the crystal and thicker at either end of the elongated crystals (Figure 11). In some places along the crystal long axes a particular zonation band grows outward perpendicular to the long axes, creating a 'bulging' morphology (Figure 4e). In elongate crystals that have such bulges, zonation appears as successive bands progressing outward from the core of the crystal and into the bulging area (Figure 4e). Older fracture calcite crystals are zoned but have no discernible zonation pattern (Figure 4d).

Energy Dispersive X-Ray Spectroscopy (EDX)

EDX elemental count maps were generated for Area '1' (Figure 4b, Figure 5a), the generation of younger veins filled with bladed calcite (measurement point every 2μm), and Area '2' (Figure 4c, Figure 5b), the older fracture generation containing wairakite and calcite (measurement point every 2μm). EDX maps of Area 1 (Figure 5a) show the same chemical zonation patterns observed in CL (Figure 4b). EDX maps of Area 2 do not show the zonation patterns observed from CL (Figure 4c). Ca and Al EDX count maps of Area 2 delineate the older wairakite vein fill from the younger calcite fill due to the differences in their chemical compositions (Figure 5b).

An EDX linescan (in weight%) of a profile across zoned calcite crystals in the younger vein generation is shown in Figure 6 next to corresponding CL and BSE images of the zonation. This plot shows that darker grey colours on the BSE image corresponds to purer calcite ($CaCO_3$), whereas lighter grey colours contain higher levels of Fe+Mn. Correlation of the linescan to the CL image shows more intricate chemical variation. Zones associated with purer $CaCO_3$ (seen on BSE image) appear as variable shades of dark red or orange CL colours. This implies additional chemical variation in these calcite crystals beyond Mn+Fe. Other major elements (O, C, Mg, Si, Al, Na) are ruled out as they display no variation after investigation by EDX. In places the Fe/Ca ratio is higher than the Mn/Ca ratio which is related to darker red CL coloured zones (~138-180 µm, 1029-1050 µm; Figure 6).

Electron Backscatter Diffraction (EBSD)

EBSD maps of calcite crystals from both the youngest and an older generation of sealed fractures are shown in Figure 7 and 9, respectively. EBSD grain maps of the younger fracture sealed by calcite mineralisation (Figure 7) show predominantly large, elongate crystals of calcite (~0.5-2 mm long), and less frequent, large, blocky calcite forms (~0.5 mm long). Smaller-sized calcite crystals (~0.05-0.25 mm) are predominantly found near the fracture walls. Elongate calcite crystals are green and blue in the IPFZ map (Figure 7b); the c-axes are at low angles to the thin section plane and perpendicular to crystal long axes (i.e. basal plane trace lies parallel to long axis). Calcite crystals with a blocky form have pink, orange, and red colours in the IPFZ map (Figure 7b) corresponding to c-axes at high angles to the thin section plane. Most elongate calcite crystals show continuous distortion (low angle ($<2°$) misorientation) along their long axes while blocky calcite crystals show no measureable internal crystal distortion (Figure 7c). Some calcite crystals (Figure 7a, 7c) have 2°-5° sub-grain boundaries (displaying rotation around the m axes), and 5°-10° sub-grain boundaries (displaying rotation around the <02-21> axis) (Figure 7d). A small number of misorientation angle boundaries of 75°-80° are observed, with rotation axes indicative of calcite e-twins ($20\bar{2}1$, Figure 7d). One point per grain calcite pole figures show calcite has a weak LPO in this fracture with the c-axes preferentially oriented perpendicular to the fracture wall. Misorientation angle distribution analyses (Figure 10a, 10b) shows little difference between random and neighbour pair misorientation angle distributions apart from a slightly higher frequency of low angle (<10°) and 75°-80° angle neighbour misorientations than the random frequency.

EBSD mapping of the older calcite vein (Figure 9) shows calcite crystals of a single orientation have grown across the fracture. Calcite crystals commonly contain either one (smaller crystals ~0.13 mm) or two twin (larger crystals, ~0.63-0.75 mm) sets and one large grain (~0.88 mm) contains three sets of twins. All twin sets in these calcite crystals are e-twins. The host calcite crystals display continuous distortion (<2°). Other host calcite microstructures, such as common 2°-5° and rare 5°-10° sub-grain boundaries, are present and have dominant <a> rotation axes (<11-20>). Misorientation angle distribution analyses (Figure 10c, 10d) shows a slightly higher frequency of low angle (<10°) neighbour misorientations than the random distribution, similar to the younger calcite vein.

Discussion

Insights into Calcite Growth in a Geothermal Fracture

The bladed calcite crystals in the younger vein investigated here do not appear to have grown following the typical symmetrical, vein-normal, growth directions expected in crack-seal fractures [Bons et al., 2012; Figure 1]. Rather the crystal morphology of this fracture implies calcite nucleated and grew outward in a number of directions with preferred crystallographic orientation, filling in available space, and eventually sealing the fracture with a 3D interlocking set of elongated crystals. The chemical zonation patterns observed in bladed calcite crystals, due to the variable inclusion of Fe and Mn into the calcite crystal structure as it precipitated, infer that they grew in a free fluid with changing composition [ten Have and Heijnen], and that they grew preferentially outward in two opposite directions (usually parallel to the fracture length) producing bladed morphologies. These observations, combined with information from EBSD texture component maps (Figure 11), and the presence of a weak calcite vein LPO, show that these elongate calcite crystals grew outward from a central core along the crystallographic m axis, such that the c-axes are perpendicular to the fracture wall. This is similar to another observation made of bladed calcite crystal growth in a geothermal well pipe, where crystals grew perpendicular to their c-axis [Tulloch, 1982], and to records of elongate calcite vein growth in other studies [Bradshaw and Phillips, 1964; González-Casado and Garcia-Cuevas, 1999; Friedman and Higgs, 2013].

Further evidence of a three-dimensional interlocking morphology for these calcite crystals are the ‘cross-cutting’ relationship that can be observed from EBSD maps (Figure 7, 11). This and other aspects of the crystal texture in this vein, such as the chemical zonation patterns, suggest that calcite precipitated and grew long in their preferred direction (parallel to the plane of the vein) and began to experience space competition in those directions. In effect, calcite growth along the fast axes became locked as growing crystals intercepted each other. This left calcite with the option of growing outward parallel to their c-axes giving the bladed crystals their often observed ‘bulge’ morphology (Figure 11). This continued, along with new calcite crystal nucleation (evidenced by small calcite crystals within the fracture), until nearly all the available fracture space was filled.

Potential models for the calcite morphology and microstructure observed in the younger vein investigated here include: growth of calcite crystals in 3D from numerous sites at the fracture wall, and calcite replacement of a pre-existing carbonate vein fill. The latter is unlikely given that bladed calcite is indicative of the near-instant, flash-sealing of hydro-fractures after they formed [Christenson, 1987]. Progressive 3D growth from a number of sites provides a more probable method to generate the observed vein texture here. The walls of the investigated vein are irregular in shape as observed from hand-specimen and thin section (Figure 3). This would have provided a number of variably oriented surfaces that allowed calcite crystals to nucleate, with some then growing rapidly along their m-axes outward and into the open fracture space, with their long-axes preferably aligned to a given surrounding stress field, while others form smaller calcite crystal clusters at the fracture wall as observed (Figure 7). Fast growing elongate calcite crystals would experience space competition with each other, growing elongate around each other, providing the interlinked bladed texture observed.

Calcite morphologies in the older vein investigated do not have the bladed morphologies observed in the younger vein. They appear to have grown across the open width of the fracture as one single crystal, implying that crystal nucleation of calcite in this fracture was syntaxial, with initial growth on the wairakite crystals on one side of the vein wall, followed by asymmetrical growth (i.e. from one wall of the fracture only). Chemical zonation in these crystals does not appear to have a discernible pattern that can be related to growth. We argue here that the calcite in this vein does not represent wairakite replacement as the thin section and SEM observations clearly show textures expected from space infilling, and previous observations that the minerals in these veins are in textural equilibrium [Christenson, 1987, Absar and Blatiner, 1985]. However, further work to determine any potential control wairakite may have on the nucleation, crystal lattice orientation, and growth development of calcite, would benefit from further EBSD study. Initial attempts to do so in this investigation were hindered due to poor EBSD indexing of the wairakite phase.

Different calcite sealing mechanisms are present in the two different veins. Discerning the dominant cause for this variation is difficult given the large number of variables associated with calcite formation in the Kawerau Geothermal Field and the limitations of currently acquired data. Possible insight may come from cathodoluminesence observations. Rate of calcite crystallisation largely controls the morphology of precipitating calcite crystals [Folk, 1974]. Fe and Mn incorporation into calcite can be affected by fluid composition [Wogelius et al., 1997], and also by calcite precipitation rates and temperature. Both the Fe and Mn content in calcite increases with decreasing precipitation rate, or increasing temperature, with the ratio of Mn/Fe increasing with decreasing precipitation rates [Dromgoole and Walter, 1990]. The observed variation in cathodoluminesence between calcite in the older and younger vein may have resulted from different precipitation rates, which influenced the style of calcite growth and thus fracture sealing. We rule out the control of temperature on cathodoluminesence here as the younger and older vein calcite is thought to have precipitated from fluids of similar temperatures [Christenson, 1987]. We note here that relationships between Fe and Mn incorporation into calcite and precipitation rates have not been tested at the geothermal fluid temperatures the calcite in this study precipitated from, and further research into that relationship is required.

Continuous lattice distortion across calcite crystals is observed in both fractures. This may indicate low levels of dislocation creep activity, enough to subtly deform the crystal lattice but not enough to create and migrate subgrain boundaries. However, simple grain growth can also generate the continuous lattice distortion observed here. Studies of the kinetics and mechanisms of carbonate/calcite growth show that for low levels of supersaturation in the precipitating fluid, {10-14} calcite face growth occurs at surface defects on the deposition surface, including screw dislocations, i.e. defect-originated growth, and at higher supersaturations growth progresses via a homogeneous surface nucleation process (Lefaucheux et al., 1973; Lefaucheux and Robert, 1977; Teng et al., 2000; Xu et al., 2014). A crystal growth explanation for the observed diffuse misorientation profiles in calcite crystals in the younger fracture is supported by its spatial correlation with calcite crystal growth directions (Figure 11). Continuous distortion is only observed in elongate calcite crystals, with crystal misorientation increasing away from the crystal core (as determined from calcite CL maps). Thus as the calcite crystal grows, becoming elongate along its preferred growth axis (the m axis), it accumulates small lattice defects that subtly alter the crystal lattice orientation. This observation infers that the bladed calcite in this vein precipitated from boiling fluids with low levels of supersaturation with respect to calcite. This model of variable crystal growth direction bears similarities to textures noted in other vein crystal growth [Urai et al., 1991; Bons, 2001], and to mineral scale build up inside autoclaves [Timms et al., 2009].

Geothermal Reservoir Conditions from Vein Calcite Deformation

Calcite crystals in both fractures contain low angle (2° - <10° misorientation) sub-grain boundaries. While these sub-grain boundaries are restricted to a few calcite crystals in the younger fracture, they are common in the calcite crystals of the older fracture. Subgrain development may be the result of deformation via dislocation creep in these calcite crystals, or, as discussed earlier, potentially a result of calcite growth incorporating surface defects. If we assume dislocation creep as the cause of subgrains in calcite we can conclude that crystals in the older fracture have undergone greater deformation than crystals in the younger fracture. Further to this, the misorientation axes of the subgrain boundaries found in the older and younger calcite crystals are different. The youngest fracture calcite has dominant *m* (for subgrain boundaries of 2-5° misorientation) and *sd* <02-21> (for subgrain boundaries of 5-<10° misorientation) rotation axes. Rotation axes are dominantly *a* in calcite in the older fracture for all subgrain boundary categories. As such we can propose that that not only has calcite in each fracture generation undergone different amounts of dislocation creep, the slip systems by which it was operating also vary. The operation of various slip systems in calcite has been shown to be temperature dependent under particular strain rates and so documenting which ones are in operation in geothermal veins can potentially inform us of deformation and thermal history of a rock (De Bresser and Spiers, 1997). Application of this theory to calcite veins in geothermal reservoirs bear further study as it may prove a useful tool for estimating the thermal evolution of the resource.

Measuring the orientation of calcite c-axes allows determination of the ‘tension’ direction the rock was under [Gonzàlez-Casado and García-Cuevas, 1999]. The calcite sealing the youngest fracture generation shows a weak LPO, with calcite c-axes aligned perpendicular to the fracture wall (Figure 13). As the sample investigated here does not have a geographical reference frame, we cannot infer the geographical extension direction associated with the formation of this fracture. We can, however, state that the extension direction during the time of calcite crystal growth in this fracture was perpendicular to the fracture length. An extension direction perpendicular to the fracture walls, in combination with the observed small, lateral offset of an older structure indicates this fracture was created through a combination of extension (mode I) and shear (mode II/III) kinematics.

Calcite crystals in both the older and younger fractures contain e-twins. Twinning density is higher in calcite crystals in the older fracture than the younger fracture. Mechanical twinning is a common microstructure in calcite and often operates as a deformation mechanism [Barber and Wenk, 1979; Burkhard, 1993; Larsson and Christy, 2008]. The relationship between calcite twin structures, temperature, and stress and strain makes them useful for determining the magnitudes and orientations of the principal stress axes in tectonic environments [Jamison and Spang, 1976; Laurent et al., 1981; Groshong Jr. et al., 1984; Rowe and Rutter, 1990; Lacombe and Laurent, 1992; Ferrill et al., 2004; Gonzàlez-Casado et al., 2006; Chen et al., 2011]. Certain twinning properties in calcite lend themselves to the determination of stress, for example, determination of strain associated with twinning can be done by measuring the average thickness of twins (the amount of simple shear deformation is proportional to the twin thickness) [Groshong, 1972; Groshong et al., 1984; Ferrill, 1991; Ferrill et al., 2004]. Additionally, paleo-differential stress magnitudes can be determined from log twin density or the percentage of calcite crystals with one, two, or three twin sets [Rowe and Rutter, 1990].

The lack of twinning in the calcite crystals of the younger vein implies that the rock has experienced little strain since this sealing event. Thus, we suggest that the fracturing represented by the bladed calcite veins, at least for the basement rock in the vicinity of well KA30, marks the last significant brittle deformation event (hydrofracturing associated with volcanic activity of nearby Putauaki). However, the low number of grains captured in this dataset, and the lack of orthogonal sections to investigate, prevents a full strain and stress analysis using calcite twins. A preliminary calculation of the log twin density of calcite crystals in the older vein is presented here in order to highlight the potential of a further, more robust study of this kind in the future. These measurements of calcite twin density do not follow the prescribed methodology in Rowe and Rutter [1990], in that twin densities are not measured from this sample on orthogonal surfaces, rather they have been calculated based on one observed section. Using EBSD maps of the older calcite vein, we measured the number of twins/mm for each calcite crystal, defined by Rowe and Rutter [1990] as the rate of change of the number of lamellae of a given twin set with respect to grain diameter measured normal to the trace of the twin lamellae. This was done for the two twin sets observed, set 1 and set 2, with set 1 representing the oldest twinning in these crystals determined from cross-cutting relationships. Differential stress magnitudes are determined from these preliminary calcite log twin density data using the Rowe and Rutter [1990] equation determined from experimental and natural data [1990], assuming that the relationship derived from their study is applicable to all naturally deformed rocks, and that the density of nuclei for twin formation is constant around calcite crystal boundaries.

Based on the log twin densities from twin set 1, calcite crystals in the older vein have experienced high differential stresses at some stage after the calcite precipitated (~200 - 250 MPa ± 43 MPa) (Figure 12). This differential stress magnitude recorded by calcite in the older vein represents a) the stress required to cause the greywacke rock to hydrofracture resulting in the formation of the younger bladed calcite vein, which may represent the last stage of brittle deformation of the basement rock in this area as discussed previously or b) possible deformation events that occurred after the calcite of the older vein has precipitated but before the hydrofracturing event that generated the younger calcite veins. Assuming that the calcite twinning in the older vein is recording the stress required to generate the younger hydrofracturing, differential stresses high enough to overcome the yield strength of the greywacke (which has UCS values ranging from 164 – 310 MPa) would be required [Richards and Read, 2007; McNamara et al., 2014]). If the twinning in the older fracture calcite is a result of this event then the recorded differential stresses of ~205 MPa seem realistic but a more robust study of the calcite twinning should be carried out before drawing any final conclusions.

Fluid Flow

Petrographic, microstructural and chemical mapping of vein fills in geothermal fractures can provide useful information on the evolution of structural permeability in the basement hosted reservoir at the Kawerau Geothermal Field. It is a general concept that progressive mineralisation within a fracture decreases the porosity and permeability of that structure, but only if it ceases to propagate and open, and assuming that fracture opening is not concurrent with mineral precipitation, in which case the structure would potentially host little permeability at all. Given that the generation of the fractures studied here is associated with disruptive, energetic hydrofracturing, it is likely they were initially open to fluid flow. Fluid flow capability of the fractures was then progressively reduced by mineral precipitation, and gradual mechanical closing of these fractures due to post hydraulic fracturing decreased fluid pressure.

It is thought that as fracture sealing minerals grow from fracture walls there is a tendency for smaller fractures to be sealed off more efficiently and quickly than larger scale fractures. This would lead to wider fractures dominating the structural permeability of a rock (Marrett and Laubach, 1997). Fast rates of bladed calcite growth (~0.1 mm/day) [Tulloch, 1982], would suggest that even wide fractures are sealed quickly. As such, wide fractures may not represent the dominant permeable structures in a geothermal system as has been suggested by other studies [Sheridan et al., 2003; Davatzes and Hickman, 2009; McLean and McNamara, 2011; Wallis et al., 2012]. Observations of the occurrence of wide aperture fractures existing outside permeable zones in geothermal wells have been noted in other studies, supporting this theory [McNamara et al., 2015; Massiot et al., 2015].

Finally, growth of bladed calcite, despite occurring at rapid rates, has the potential to act as a mechanism by which to preserve or prolong the permeable lifetime of the hydraulic fractures observed at Kawerau. Our microstructural and chemical investigation of bladed calcite crystals shows they can grow quickly from fracture walls to create a complex 3D interlocking structure. Rapid growth of this calcite crystal morphology may serve to prop open these wide fractures, acting against their tendency to close. By propping open the hydraulic fractures, longer time periods of fluid flow are supported until eventually calcite precipitation fills up all available space.

Conclusions

Observations of calcite crystal morphology, chemical zonation, and crystallographic patterns from two sealed geothermal fractures show different fracture sealing mechanisms in operation; asymmetrical syntaxial growth, and growth in free 3D space. Examination of a larger set of calcite fractures will be required to determine if a preferred calcite sealing mechanism exists in geothermal veins, and whether the sealing mechanisms is dependent on the how the calcite precipitates (e.g. whether boiling conditions are present at the time of calcite growth).

Combined EBSD/EDX/CL study of calcite sealed fractures in geothermal reservoirs shows promise as a useful tool in understanding its evolution:

- Lattice distortion associated with the continual growth of bladed calcite crystals may indicate defect-originated growth. This provides insight into the geothermal fluid conditions that precipitated these crystals as this type of calcite growth occurs from lower levels of supersaturation.
- The lack of significant twinning and micro-deformation (sign of deformation) in the bladed calcite of the youngest fracture generation implies that this fracture represents the most recent tectonic event strong enough to create new fractures in the basement. The low occurrence of twinning also implies that since this fracture was sealed there

has been little strain accumulation in the rock, or if there has none of it is accommodated by the calcite in this fracture.

- Observations of calcite twinning in older calcite filled fractures may potentially record differential stress magnitudes that this reservoir rock has been subjected to over time. A more in-depth study with appropriate orthogonal sections of these calcite filled fractures is required to obtain more accurate data.
- Determination of calcite lattice preferred orientations from sealed fractures can provide insight into the tension direction of the structure and possible variation in the orientation of tension over time.

Acknowledgements

Acknowledgements go to the Geothermal Resources of New Zealand research program at GNS Science and the University of Otago for funding for this work, Ngati Tuwharetoa Geothermal Assets (NGTA) for supplying core samples from Kawerau Geothermal Field and for permission to release this data.

References

Absar, A., P. Blattner (1985), Successive hydrothermal events, as indicated by oxygen isotope composition and petrography of greywacke basement rocks, Kawerau Geothermal Field, New Zealand, *Proceedings 7th New Zealand Geothermal Workshop*.

Absar, A. (1988), Oxygen isotope and hydrothermal alteration studies at Kawerau and Ohaaki-Broadlands geothermal fields, New Zealand, Ph.D. Thesis, University of Auckland, New Zealand.

Adams, C.J., N. Mortimer, H. J. Campbell and W. L. Griffin (2009), Age and isotropic characterisation of metasedimentary rocks from the Torlesse Supergroup and Waipapa Group in the central North Island, New Zealand, *New Zealand Journal of Geology and Geophysics, 52*, 149-170.

André, L., V. Rabemanana, F. –D. Vuataz (2006), Influence of water-rock interactions on fracture permeability of the deep reservoir at Soultz-sous-Forêts, France, *Geothermics, 35,* 507-531.

Asanuma, H., N. Soma, H. Kaieda, Y. Kumano, T. Izumi, K. Tezuka, H. Niitsuma and D. Wyborn (2005), Microseismic monitoring of hydraulic stimulation at the Australian HDR Project in Cooper Basin, *Proceedings World Geothermal Congress 2005*.

Barker, S. L. L., S. F. Cox, S. M. Eggins and M. K. Gagan (2006), Microchemical evidence for episodic growth of antitaxial veins during fracture-controlled fluid flow, *Earth and Planetary Science Letters, 250*, 331-344, DOI: 10.1016/j.epsl.2006.07.051.

Barker, S. L. L., V. C. Bennett, S. F. Cox, M. D. Norman and M. K. Gagan (2009), Sm-Nd, Sr, C and O isotope systematics in hydrothermal calcite-fluorite veins: Implications for fluid-rock reaction and geochronology, *Chemical Geology, 268*, 58-66, doi:10.1016/j.chemgeo.2009.07.009.

Batzle, M.L., G. Simmons (1976), Microfractures in rocks from two geothermal areas, *Earth and Planetary Science Letters, 30*, 71-93.

Begg, J. G. and V. Mouslopoulou (2010), Analysis of late Holocene faulting within an active rift using lidar, Taupo Rift, New Zealand, *Journal of Volcanology and Geothermal Research*, *190*, 152-167, doi:10.1016/j.jvolgeores.2009.06.001.

Bertani, R. (2012), Geothermal power generation in the world 2005–2010 update report, *Geothermics, 41*, 1–29, doi:10.1016/j.geothermics.2011.10.001 .

Bestmann, M., Prior, D.J. (2003) Intragranular dynamic recrystallization in naturally deformed calcite marble: diffusion accommodated grain boundary sliding as a result of subgrain rotation recrystallization, Journal of Structural Geology, 25, 1597-1613.

Bibby, H.M., T. Caldwell, F. Davey and T. Webb (1995), Geophysical evidence on the structure of the Taupo Volcanic Zone and its hydrothermal circulation, *Journal of Volcanology and Geothermal Research, 68*, 29–58, doi:10.1016/0377-0273(95)00007-H.

Bignall, G. and S. D. Milicich (2012), Kawerau Geothermal Field: geological framework. *GNS Science Consultancy Report 2012/118*, Institute of Geological & Nuclear Sciences, Lower Hutt, New Zealand.

Blackwell, D. D., P. T. Negraru and M. C. Richards (2007), Assessment of the enhanced geothermal system resource base of the United States, *Natural Resources Research, 15*, 283–308, doi:10.1007/s11053-007-9028-7.

Bons, P. D., (2001), Development of crystal morphology during unitaxial growth in a progressively widening vein: I. The numerical model, *Journal of Structural Geology, 23*, 865-872, doi:10.1016/S0191-8141(00)00159-0.

Bons, P. D., M. A. Elburg and E. Gomez-Rivas (2012), A review of the formation of tectonic veins and their microstructure, *Journal of Structural Geology, 43*, 33-62.

Brace, W. F. (1980), Permeability of crystalline and argillaceous rocks, *International Journal of Rock Mechanics and Mining Sciences & Geomechanics Abstracts, 17*, 241–251, doi:10.1016/0148-9062(80)90807-4.

Bradshaw, R. and F. C. Phillips (1964), X-ray studies of natural fabrics. I. Growth-fabrics in hematite kidney ore and in fibrous calcite, *Mineralogical Magazine, 36*, 70-77.

Browne, P.R.L. (1978) Hydrothermal alteration in active geothermal fields, *Annual Review of Earth and Planetary Sciences, 6,* 229-250, doi:10.1146/annurev.ea.06.050178.001305.

Burkhard, M. (1993) Calcite twins, their geometry, appearance and significance as stress-strain markers and indicators of tectonic regime: a review, *Journal of Structural Geology, 15,* 351-368.

Chambefort, I., Lewis, B., Wilson, C.J.N., Rae, A.J., Coutts, C., Bignall, G., Ireland, T.R. (2014), Stratigraphy and structure of the Ngatamariki geothermal system from new zircon U-Pb geochronology: Implications for Taupo Volcanic Zone evolution, *Journal of Volcanology and Geothermal Research, 274*, 51-70, doi: 10.1016/j.jvolgeores.2014.01.015.

Chen, K., Kunz, M., Tamura, N., Wenk, H.-R. (2011) Deformation twinning and residual stress in calcite studied with synchrotron polychromatic X-ray microdiffraction, *Physics and Chemistry of Minerals, 38*, 491-500.

Christenson, B. W. (1987), Fluid - mineral equilibria in the Kawerau hydrothermal system, Taupo Volcanic Zone, New Zealand, Ph.D. Thesis, University of Auckland, New Zealand.

Christenson, B. W. (1997), Kawerau Geothermal Field: Geochemical structure of the reservoir and its response to exploitation, *Transactions of the Geothermal Resources Council, 21*, 17-24.

Cole, J. W. and K. D. Spinks (2009), Caldera volcanism and rift structure in the Taupo Volcanic Zone, New Zealand, *Geological Society, London, Special Publications, 327*, 9–29, doi:10.1144/SP327.2.

Cox, S. F. and M. A. Etheridge (1983), Crack-seal fibre growth mechanisms and their significance in the development of oriented layer silicate microstructures, *Tectonophysics , 92*, 147-170, doi:10.1016/0040-1951(83)90088-4.

Davatzes, N. C. and S. H. Hickman (2010), Stress, fracture, and fluid-flow analysis using acoustic and electrical image logs in hot fractured granites of the Coso Geothermal Field, California, U.S.A., in Dipmeter and borehole image log technology, edited by M. Pöppelreiter, C. García-Carballido and M. Kraaijveld, *AAPG Memoir, 92*, 259-293, doi:10.1306/13181288M923134.

Davatzes, N. C. and S. H. Hickman (2009), Fractures, stress and fluid flow prior to stimulation of well 27-15, Desert Peak, Nevada, EGS Project, *Proceedings, 34th Workshop on Geothermal Reservoir Engineering*.

De Bresser, J. H. P. and C. J. Spiers (1997), Strength characteristics of the *r*, *f*, and *c* slip systems in calcite, *Tectonophysics, 272*, 1-23, doi:10.1016/S0040-1951(96)00273-9.

Dempsey, D., J. Rowland, R. Archer (2012), Modelling geothermal fluid flow and silica deposition along an active fault, *Proceedings, 37th Workshop on Geothermal Reservoir Engineering*.

Dezayes, C., A. Genter and B. T. Valley (2010), Structure of the low permeable naturally fractured geothermal reservoir at Soultz, *Comptes Rendus Geoscience, 342*, 517–530, doi:10.1016/j.crte.2009.10.002.

Dobson, P. F., T. J. Kneafsey, J. Hulen and A. Simmons (2003), Porosity, permeability, and fluid flow in the Yellowstone geothermal system, Wyoming, *Journal of Volcanology and Geothermal Research, 123,* 313-324.

Dromgoole, E. L. and L. M. Walter (1990), Iron and manganese incorporation into calcite: Effects of growth kinetics, temperature and solution chemistry, *Chemical Geology, 81*, 311-336.

Durney, D. W. and J. G. Ramsay (1973), Incremental strains measured by syntectonic crystal growths, in Gravity and Tectonics, edited by K. A. De Jong and R. Scholten, 67-96.

Ferrill, D. A. (1991), Calcite twin widths and intensities as metamorphic indicators in natural low-temperature deformation of limestone, *Journal of Structural Geology, 13*, 667-675, doi: 10.1016/0191-8141(91)90029-I.

Ferrill, D. A., A. P. Morris, M. A. Evans, M. Burkhard, R. H. Groshong Jr. and C. M. Onasch (2004), Calcite twin morphology: a low-temperature deformation geothermometer, *Journal of Structural Geology, 26*, 1521-1529, doi:10.1016/j.jsg.2003.11.028.

Folk, R. L. (1974), The natural history of crystalline calcium carbonate: Effect of magnesium content and salinity, *Journal of Sedimentary Petrology, 44*, 40-53.

Fournier, R. O. (1985), Carbonate transport and deposition in the epithermal environment, *Reviews in Economic Geology, 2*, 63-71.

Friedman, M. and N. G. Higgs (1981), Calcite Fabrics in Experimental Shear Zones, in Mechanical Behaviour of Crustal Rocks: The Handin Volume, edited by N.L. Carter, M. Friedman, J.M. Logan and D.W. Stearns, American Geophysical Union, Washington, D. C., doi:10.1029/GM024p0011.

Genter, A., H. Traineau (1996), Analysis of macroscopic fractures in granite in the HDR geothermal well EPS-1, Soultz-sous-Forêts, France, *Journal of Volcanology and Geothermal Research, 72*, 121-141.

Genter, A., K. Evans, N. Cuenot, D. Fritsch, B. Sanjuan (2010), Contribution of the exploration of deep crystalline fractured reservoir of Soultz to the knowledge of enhanced geothermal systems (EGS), *Competes Rendus Geoscience, 342*, 502-516.

González-Casado, J. M. and C. García-Cuevas (1999), Calcite twins from microveins as indicators of deformation history, *Journal of Structural Geology, 2*1, 875-889, doi:10.1016/S0191-8141(99)00081-4.

Groshong, R. H. (1972), Strain calculated from twinning in calcite, *Geological Society of America Bulletin, 83*, 2025-2038, doi:10.1130/0016-7606(1972)83[2025:SCFTIC]2.0.CO;2.

Groshong, R. H., L. W. Teufel and C. Gasteiger (1984), Precision and accuracy of the calcite strain-gage technique, *Geological Society of America Bulletin, 95*, 357-363, doi:10.1130/0016-7606(1984)95<357:PAAOTC>2.0.CO;2.

Halfpenny, A. (2010), Some important practical issues for the collection and manipulation of electron backscatter diffraction (EBSD) data from geological samples, *Journal of the Virtual Explorer, 35*, doi: 10.3809/jvirtex.2011.00272.

Hébert, R. L., B. Ledésert, A. Genter, D. Bartier, C. Dezayes (2011), Mineral precipitation in geothermal reservoir: The study case of calcite in the Soultz-sous-Forêts enhanced geothermal system, *Proceedings, Thirty-Sixth Workshop on Geothermal Reservoir Engineering, SGP-TR-191.*

Hedenquist, J. W., R. W. Henley (1985), Effect of CO2 on freezing point depression measurements of fluid inclusions - evidence from active systems and implications for epithermal mineralization, *Economic Geology, 80*, 1379-1406.

Hedenquist, J. W. (1990), The thermal and geochemical structure of the Broadlands-Ohaaki geothermal system, New Zealand, *Geothermics, 19*, 151-185.

Hilgers, C., D. Koehn, P. D. Bons and J. L. Urai (2000), Development of crystal morphology during unitaxial growth in a progressively widening vein: II. Numerical simulations of the evolution of antitaxial fibrous veins, *Journal of Structural Geology, 23*, 873-885, doi:10.1016/S0191-8141(00)00160-7.

Hilgers, C., K. Dilg-Gruschinski and J. L. Urai (2004), Microstructural evolution of syntaxial veins formed by advective flow, *Geology, 32*, 261-264.

Hurst, A. W., H. M. Bibby and R. R. Robinson (2002), Earthquake focal mechanisms in the central Taupo Volcanic Zone and their relation to faulting and deformation. *New Zealand Journal of Geology and Geophysics, 45*, 527–536, doi:10.1080/00288306.2002.9514989.

Hurst, T., S. Bannister, R. Robinson and B. Scott (2008), Characteristics of three recent earthquake sequences in the Taupo Volcanic Zone, New Zealand. *Tectonophysics 452*, 17– 28, doi:10.1016/j.tecto.2008.01.017.

Krupp, R. E. and T. M. Seward (1987), The Rotokawa geothermal system, New Zealand; an active epithermal gold-depositing environment, *Economic Geology, 82*, 1109–1129, doi:10.2113/gsecongeo.82.5.1109.

Lacombe, O. and P. Laurent (1992), Determination of principal stress magnitudes using calcite twins and rock mechanics data, *Tectonophysics, 202*, 83-93, doi:10.1016/0040-1951(92)90456-G.

Lefaucheux, F., M. C. Robert and A. Authier (1973), Étude des défauts créés lors de perturbations extérieures imposées au cours de la croissance hydrothermale de calcite, *Journal of Crystal Growth, 19*, 329-337, doi:10.1016/0022-0248(73)90057-2.

Lefaucheux, F. and M. C. Robert (1977), Defects revealing two growth processes for a face case of hydrothermal synthetic calcite, *Journal of Crystal Growth, 38*, 29-37, doi:10.1016/0022-0248(77)90369-4.

Leonard, G. S., J. G. Begg and C. J. N. Wilson (2010), Geology of the Rotorua area: scale 1:250,000, *Institute of Geological & Nuclear Sciences 1:250,000 geological map 5*, Institute of Geological & Nuclear Sciences Limited, Lower Hutt, New Zealand.

Litchfield, N. J., R. Van Dissen, R. Sutherland, P. M. Barnes, S. C. Cox, R. Norris, R. J. Beavan, R. Langridge, P. Villamor, K. Berryman, M. Stirling, A. Nicol, S. Nodder, G. Lamarche, D. J. A. Barrell, J. R. Pettinga, T. Little, N. Pondard, J. J. Mountjoy and K. Clark (2014), A model of active faulting in New Zealand, *New Zealand Journal of Geology and Geophysics, 57*, 32-56, doi:10.1080/00288306.2013.854256.

Marrett, R. and Laubach, S. E. (1997), Diagenetic controls on fracture permeability and sealing, *International Journal of Rock Mechanics and Mining Sciences, 34*.

Massiot, C., McNamara, D. D., Nicol, A., Townend, J., (2015), Fracture width and spacing distributions from borehole televiewer logs and core in the Rotokawa Geothermal Field, New Zealand, *Proceedings World Geothermal Congress 2015*.

McLean K. and D. D. McNamara (2011), Fractures interpreted from acoustic formation imaging technology: correlation to permeability, *Proceedings, Thirty-Sixth Workshop on Geothermal Reservoir Engineering*, SGP-TR-191.

McNamara, D. D., D. Faulkner and E. McCarney (2014), Rock properties of greywacke basement hosting geothermal reservoirs, New Zealand: Preliminary results, *Proceedings, Thirty-Ninth Workshop on Geothermal Reservoir Engineering,* SGP-TR-202.

McNamara, D. D., Massiot, C., Lewis, B. and Wallis, I. C. (2015), Heterogeneity of structure and stress in the Rotokawa Geothermal Field, New Zealand, *Journal of Geophysical Research, 120*, 1243-1262, doi: 10.1002/2014JB011480.

Milicich, S. D., C. J. N. Wilson, G. Bignall, B. Pezaro, C. Bardsley (2013), Reconstructing the geological and structural history of an active geothermal field: A case study from New Zealand, *Journal of Volcanology and Geothermal Research, 262*, 7-24, doi:10.1016/j.jvolgeores.2013.06.004.

Milicich, S. D., C. Bardsley, G. Bignal, C. J. N. Wilson (2014), 3-D interpretive modelling applied to the geology of the Kawerau geothermal system, Taupo Volcanic Zone, New Zealand, *Geothermics, 51*, 344-350.

Nairn, I. A., S. Beanland (1989), Geological setting of the 1987 Edgecumbe earthquake, New Zealand, *New Zealand Journal of Geology and Geophysics, 32*, 1-13.

Nairn, I. A. (2002), Geology of the Okataina Volcanic Centre: scale 1:50,000, *Institute of Geological & Nuclear Sciences geological map 25*, Institute of Geological & Nuclear Sciences Limited, Lower Hutt, New Zealand.

Nicol, A., J. Walsh, K. Berryman and P. Villamor (2006), Interdependence of fault displacement rates and paleoearthquakes in an active rift, *Geology, 34*, 865 doi:10.1130/G22335.1.

Nord, G.L. (1994) Transformation-induced twin boundaries in minerals, *Phase Transitions, 48*, 107-134.

Nüchter J. –A. and B. Stöckhert (2007), Vein quartz microfabrics indicating progressive evolution of fractures into cavities during postseismic creep in the middle crust, *Journal of Structural Geology, 29*, 1445-1462.

Okamoto, A. and K. Sekine (2011), Texture of syntaxial quartz veins synthesized by hydrothermal experiments, *Journal of Structural Geology, 33*, 1764-1775.

Phillips, W. J. (1972), Hydraulic fracturing and mineralization, *Journal of the Geological Society of London, 128*, 337-359.

Piazolo, S., Prior, D.J., Holness, M.D. (2005) The use of combined cathodoluminescence and EBSD analysis: a case study investigating grain boundary migration mechanisms in quartz, *Journal of Microscopy, 217*, 152-161, doi: 10.1111/j.1365-2818.2005.01423.x.

Prior, D. J., P. W. Trimby and U. D. Weber (1996), Orientation contrast imaging of microstructures in rocks using forescatter detectors in the scanning electron microscope, *Mineralogical Magazine, 60,* 859-869.

Prior D. J., A. P. Boyle, F. Brenker, M. C. Cheadle, A. Day, G. Lopez, L. Peruzzo, G. J. Potts, S. Reddy, R. Spiess, and N. E. Timms (1999), The application of electron backscatter diffraction and orientation contrast imaging in the SEM to textural problems in rocks, *American Mineralogist, 84,* 1741-1759.

Ramsay, J. G. (1980), The crack-seal mechanism of rock deformation, *Nature, 284*, 135-139, doi:10.1038/284135a0.

Richards, L. and S. A. L. Read (2007), New Zealand greywacke characteristics and influences on rock mass behaviour, *11th Congress of the International Society for rock Mechanics*.

Rowe, K. J. and E. H. Rutter (1990), Palaeostress estimation using calcite twinning: experimental calibration and application to nature, *Journal of Structural Geology, 12*, 1-17.

Rowland, J. V. and S. F. Simmons (2012), Hydrologic, magmatic, and tectonic controls on hydrothermal flow, Taupo Volcanic Zone, New Zealand: Implications for the formation of epithermal vein deposits, *Economic Geology, 107*, 427–457, doi:10.2113/econgeo.107.3.427.

Sausse, J., M. Fourar and A. Genter (2006), Permeability and alteration within the Soultz granite inferred from geophysical and flow log analysis, *Geothermics, 35*, 544–560, doi:10.1016/j.geothermics.2006.07.003.

Seebeck, H., A. Nicol, P. Villamor, J. Ristau and J. Pettinga (2014), Structure and kinematics of the Taupo Rift, New Zealand, *Tectonics*, 33, doi:10.1002/2014TC003569.

Sheridan, J., Kovac, K., Rose, P. E., Barton, C., McCulloch, J., Berard, B., Moore, J. M., Petty, S., Spielman, P., (2003), In situ stress, fracture and fluid flow analysis – East flank of the Coso Geothermal Field, *Proceedings, Twenty-Eighth Workshop on Geothermal Reservoir Engineering*, SGP-TR-173.

Simmons, S. F. and B. W. Christenson (1994), Origins of calcite in a boiling geothermal system, *American Journal of Science, 294*, 361-400.

Steiner, A. (1955), Wairakite, the calcium analogue of analcime, a new zeolite mineral, *Mineralogical Magazine, 30*, 691-698.

ten Have, T. and W. Heijnen (1985), Cathodoluminescence activation and zonation in carbonate rocks: an experimental approach, *Geologie en Mijnbouw, 64*, 297–310.

Teng, H. H., P. M. Dove and J. J. De Yoreo (2000), Kinetics of calcite growth: Surface processes and relationships to macroscopic rate laws, *Geochimica et Cosmochimica Acta, 64*, 2255-226, doi:10.1016/S0016-7037(00)00341-0.

Timms, N. E., J. Li and S. M. Reddy (2009), Quantitative microstructural characterization of natrojarosite scale formed during high-pressure acid leaching of lateritic nickel ore. *American Mineralogist, 94*, 1111-1119, doi:10.2138/am.2009.3104 .

Townend, J., S. Sherburn, R. Arnold, C. Boese, C. and L. Woods (2012), Three-dimensional variations in present-day tectonic stress along the Australia–Pacific plate boundary in New Zealand, *Earth and Planetary Science Letters, 353-354*, 47–59, doi:10.1016/j.epsl.2012.08.003.

Tulloch, A. J. (1982), Mineralogical observations on carbonate scaling in geothermal wells at Kawerau and Broadlands, *Proceedings 4th New Zealand Geothermal Workshop*.

Urai, J. L., P. F. Williams and H. L. M. van Roermund (1991), Kinematics of crystal growth in syntectonic fibrous veins, *Journal of Structural Geology, 13*, 823-836, doi:10.1016/0191-8141(91)90007-6.

Villamor, P. and K. R. Berryman (2001), A late Quaternary extension rate in the Taupo Volcanic Zone, New Zealand, derived from fault slip data, *New Zealand Journal of Geology and Geophysics, 44*, 243-269, doi:10.1080/00288306.2001.9514937.

Villamor, P., K. R. Berryman, I. A. Nairn, K. Wilson, N. Litchfield and W. Ries (2011), Associations between volcanic eruptions from Okataina volcanic centre and surface rupture of nearby active faults, Taupo rift, New Zealand: insights into the nature of volcano-tectonic interactions, *Geological Society of America Bulletin, 123*, 1383-1405.

Wallace, L. M., J. Beavan, R. McCaffrey and D. Darby (2004), Subduction zone coupling and tectonic block rotations in the North Island, New Zealand, *Journal of Geophysical Research, 109*, 1978-2012, doi:10.1029/2004JB003241.

Wallis, I. C., D. D. McNamara, J. Rowland and C. Massiot (2012), The nature of fracture permeability in the basement greywacke at Kawerau Geothermal Field, New Zealand, *Proceedings, Thirty-seventh Workshop on Geothermal Reservoir Engineering*, SGP-TR-194.

Wilson, C. J. N., B. F. Houghton, M. O. McWilliams, M. A. Lanphere, S. D. Weaver and R. M. Briggs (1995), Volcanic and structural evolution of the Taupo Volcanic Zone, New Zealand: a review, *Journal of Volcanology and Geothermal Research, 68*, 1-28, doi:10.1016/0377-0273(95)00006-G.

Wiltschko, D. V. and J. W. Morse (2001), Crystallization pressure versus “crack seal” as the mechanism for banded veins, *Geology, 29*, 79-82, DOI: 10.1130/0091-7613(2001) 029<0079:CPVCSA>2.0.CO;2.

Wogelius, R. A., D. G. Fraser, G. R. Wall and G. W. Grime (1997), Trace element and isotopic zonation in vein calcite from the Mendip Hills, UK, with spatial-process correlation analysis, *Geochimica et Cosmochimica Acta*, *61*, 2037-2051.

Wood, C. P., R. L. Brathwaite and M. D. Rosenberg (2001), Basement structure, lithology and permeability at Kawerau and Ohaaki geothermal fields, New Zealand, *Geothermics, 30*, 461-481, doi:10.1016/S0375-6505(01)00003-7.

Xu, M., L. Kovarik, B. W. Arey, A. R. Felmy, K. M. Rosso and S. Kerisit (2014), Kinetics and mechanisms of cadmium carbonate heteroepitaxial growth at the calcite (10-14) surface, *Geochimica et Cosmochimica Acta, 134*, 221-233, doi:10.1016/j.gca.2013.11.036.

Figure 1 Schematic models of various fracture sealing processes; a) syntaxial sealing, b) antitaxial sealing, c) stretching vein showing both delocalised vein growth (via fracture propagation through wall rock) and localised vein growth (fracture propagation across already deposited material), and d) vein formation from a pressure shadows/fringe occurring next to a rigid object.

Figure 2 Map of the Taupo Volcanic Zone showing the major structural features and the location of the Kawerau Geothermal Field. Inset provides geographical context within New Zealand.

Figure 3 a) Photograph of drill-core sample of greywacke reservoir rock from the Kawerau Geothermal Field used for study, b) Plane polarised, light microscopy image of the drill core sample. Red boxes outline individual areas selected for focused examination using CL, EDX, and EBSD, c) Cross polarised light microscopy image of the calcite vein from Area 1, d) Cross polarised light microscopy image of the calcite/wairakite vein from Area 2.

Figure 4 Cathodoluminescence (CL) images of fractured greywacke reservoir rock from Kawerau Geothermal Field. a) CL image showing cross-cutting calcite and wairakite filled veins. Inset white boxes define areas of zoom in Figure 4b and 4c, b) CL image of a bladed calcite filled vein from the youngest fracture generation. Inset dashed white box represents area of zoom in Figure 4e, c) CL image of a calcite/wairakite filled vein cross-cut by a younger calcite filled vein (white lines mark older generation fracture edges), inset white dashed box represents area of zoom in Figure 4d.

Figure 5 a) Fe and Mn EDX count maps of bladed calcite crystals in the younger generation fracture (zone 1 in Figure 3). White lines define the edge of the fracture. b) Ca and Al EDX count maps of a calcite and wairakite sealed older generation fracture (Zone 2 in Figure 3). The dashed white line defines where the older generation fracture is cross-cut by the younger generation fracture.

Figure 6 EDX data from a linescan (dashed white line shown in figure 4b) across chemically zoned, bladed calcite crystals sealing the younger fracture generation. Fe, Ca, and Mn element wt% linescan data are plotted as Fe/Ca, Mn/Ca, and Fe+Mn/Ca ratios, such that when ratio = 0, calcite is pure $CaCO_3$ (with respect to Fe and Mn), and when the ratio > 0 there is higher Fe and Mn content in the calcite. a) Graph showing variation in Mn/Ca and Fe/Ca ratios, b) Graph showing variation in Fe+Mn/Ca ratio, c) CL microscopy image of calcite crystals in the younger fracture generation across which linescan data was collected and d) the same area under as a back scattered electron image.

Figure 7 EBSD data on calcite fracture fill from the youngest generation of fracturing. a) Band Contrast map with Grain Boundary overlay, b) Band Contrast map with an Inverse Pole Figure colour scale in the sample's Z direction and Grain Boundary overlay, c) Misorientation profiles of Grains 1 and 2 (labelled in 7b) following direction indicated by red arrows, insets are Band Contrast maps with Texture Component overlays for the crystals being profiled (crystal colour indicates amount of misorientaion from a given orientation on the crystal (blue = 0°, red = 10°), d) Contoured inverse pole figures for neighbouring calcite misorientations of 2°-5°, 5°-10°, and 75°-80°.

Figure 8 Contoured pole figures of calcite crystal orientations in the younger generation fracture using one orientation measurement per calcite crystal (point per grain) for 1168 crystals. Pole figures are equal area projection, upper hemispheres and are contoured with a half width of 15° and a cluster size of 5° (Halfpenny, 2010).

Figure 9 EBSD data on calcite fracture fill from an older generation of fracturing. a) Band Contrast map with Grain Boundary overlay, b) Band Contrast map with

Inverse Pole Figure (RGB colour scale) and Grain Boundary overlay, c) Misorientation profile of Grain 1 (labelled in 8b) following direction indicated by red arrow, inset is Band Contrast map with Texture Component overlays for the crystal being profiled (colour indicates amount of misorientaion from a given orientation on the crystal; blue = 0°, red = 10°), d) Contoured inverse pole figures for neighbouring calcite misorientations of 2°-5°, 5°-10°, and 75°-80°.

Figure 10 Misorientation angle distribution analyses. Frequencies of misorientation angles for neighbour and random pair points for the younger calcite filled fracture showing a) relative frequency, and b) cumulative frequency. Frequencies of misorientation angles for neighbour and random pair points for the older calcite filled fracture showing c) relative frequency, and d) cumulative frequency.

Figure 11 a) CL images of two elongate, bladed calcite crystals from the younger fracture generation, b) EBSD texture component maps of the same two calcite crystals, c) schematic of the same crystals showing their fast growth direction (green arrows) and slower growth directions (red arrows). Red dots mark point where texture component map misorientations are scaled from, black lines = >10° misorientation boundaries (grain boundaries), purple lines = calcite twin boundaries, and yellow lines = sub-grain boundaries (2 - 5° misorientation).

Figure 12 Graph showing the determined relationship between differential stress and the log number of twins/mm in calcite crystals (from Rowe and Rutter, 1990) with two of the twin sets densities observed from calcite crystals in the older generation, wairakite/calcite sealed fracture.

Figure 13 Plane polarised light microscopy picture of the younger generation fracture sealed with bladed calcite. Inset is a contoured pole figure of the orientations of calcite crystal’s c-axes (using one orientation point per crystal) within the dashed box (Area 1). Red arrows show the preferred orientation of the c-axes on the pole figure and the direction of extension on the photograph (determined from the c-axes preferred orientation).

Figure
Click here to download high resolution image

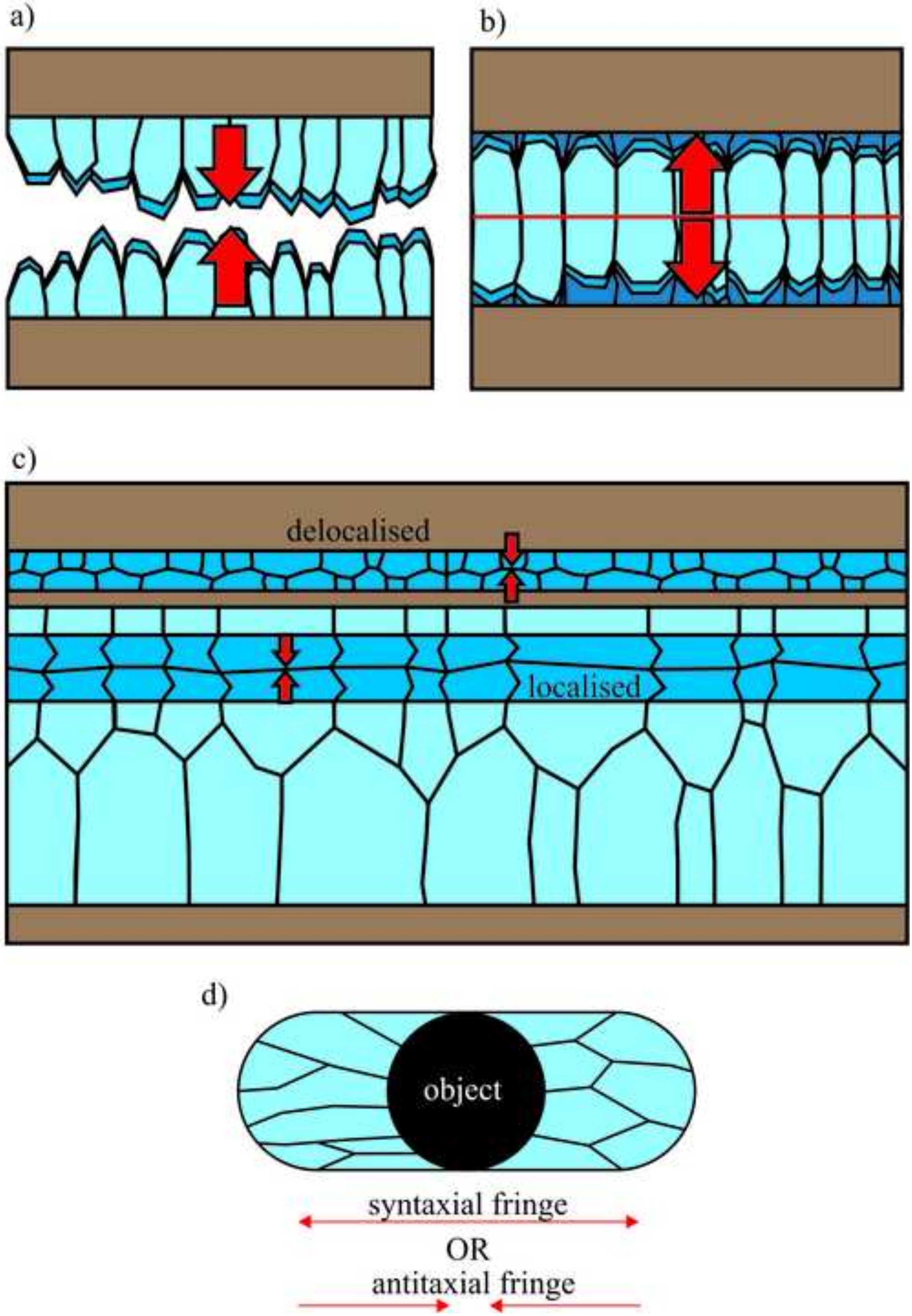

Figure

Click here to download high resolution image

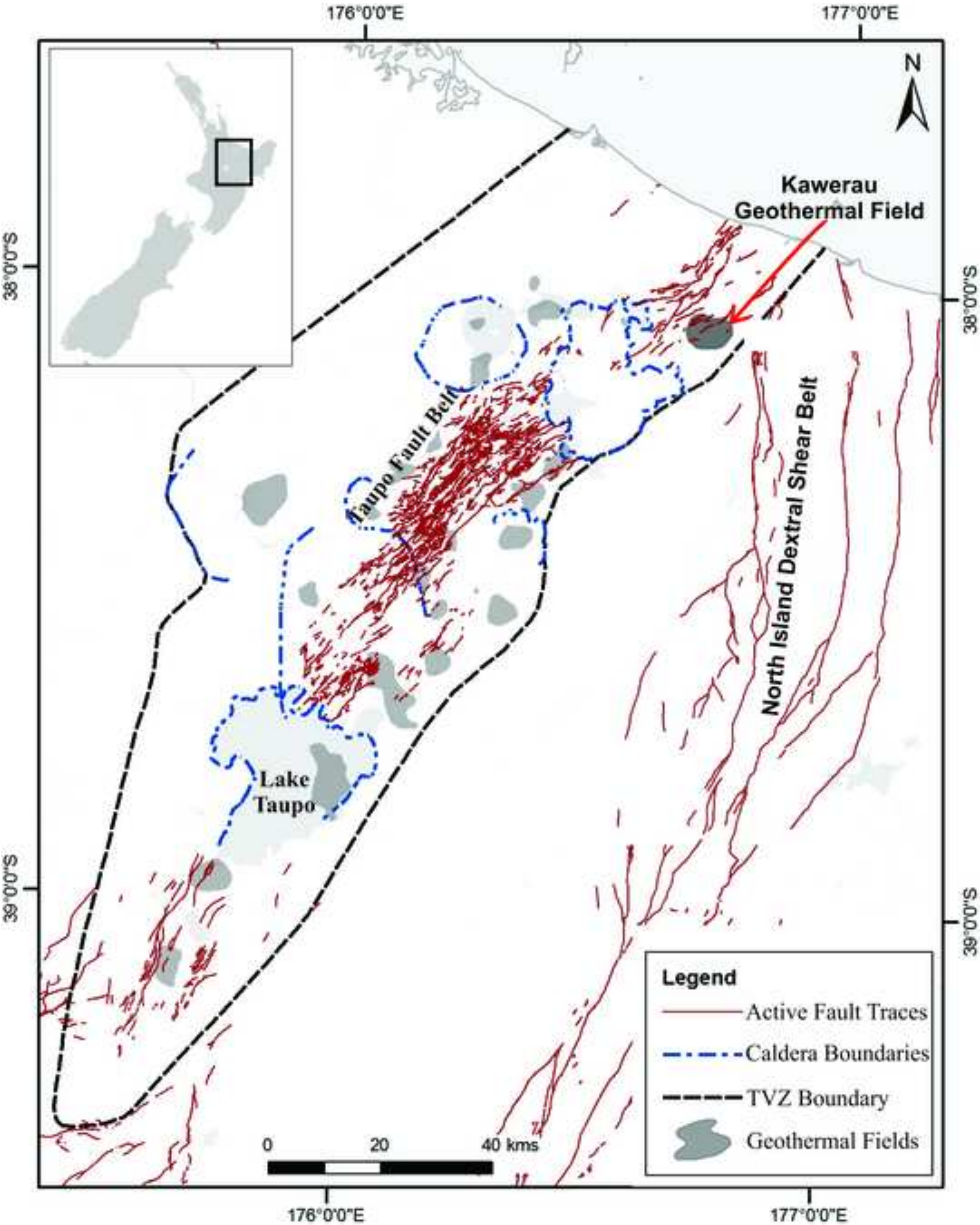

Figure
Click here to download high resolution image

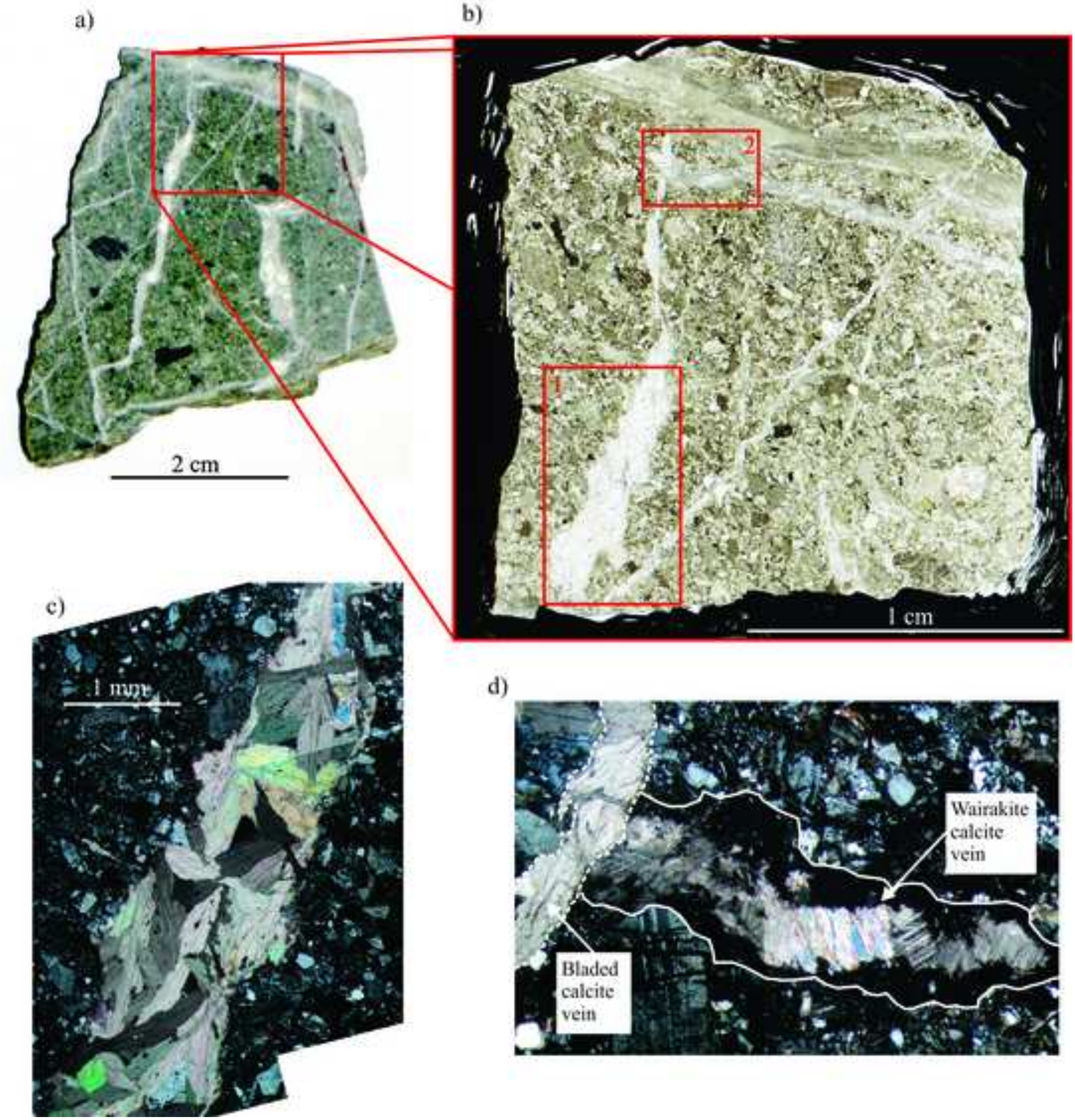

Figure
Click here to download high resolution image

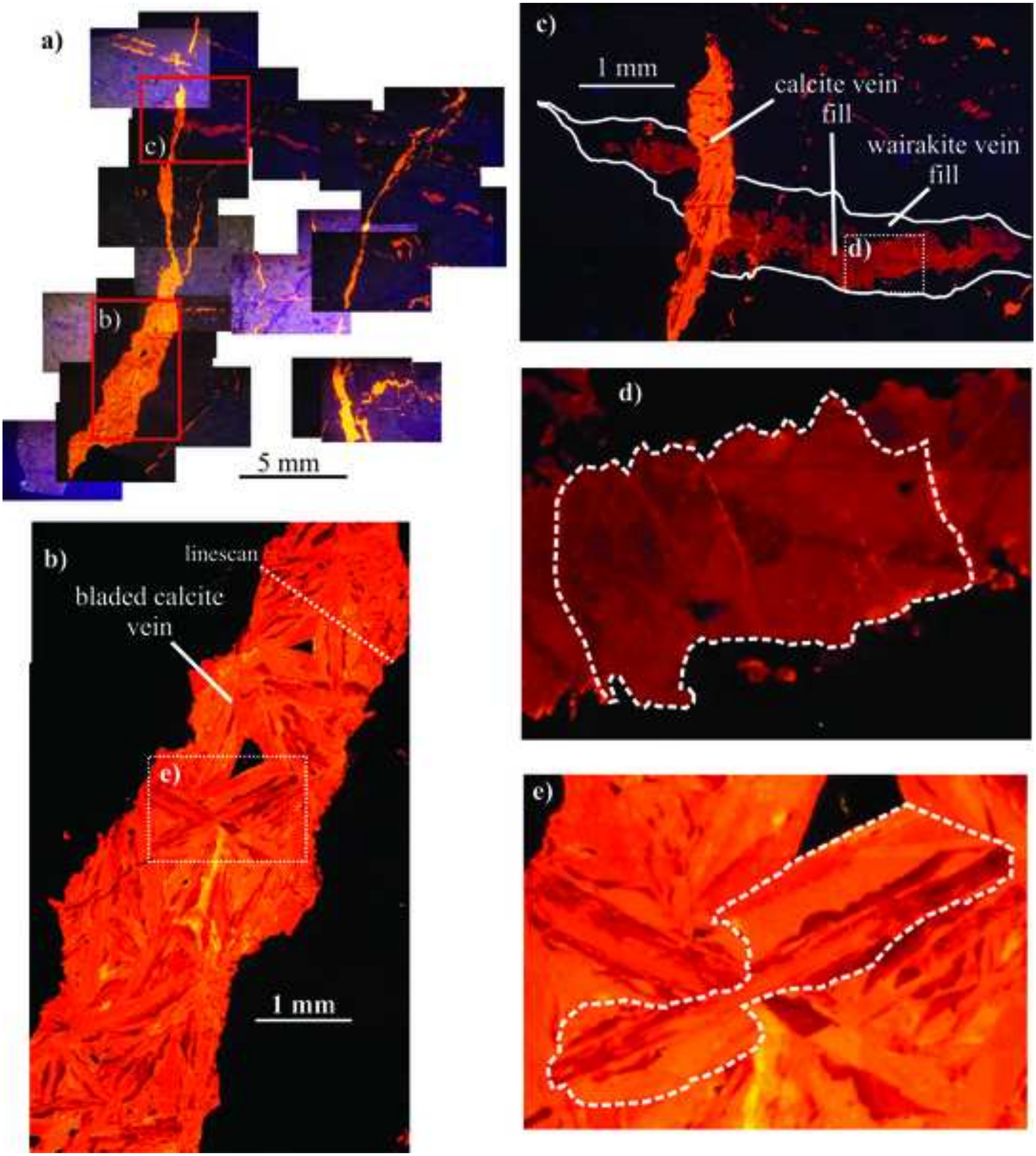

Figure
Click here to download high resolution image

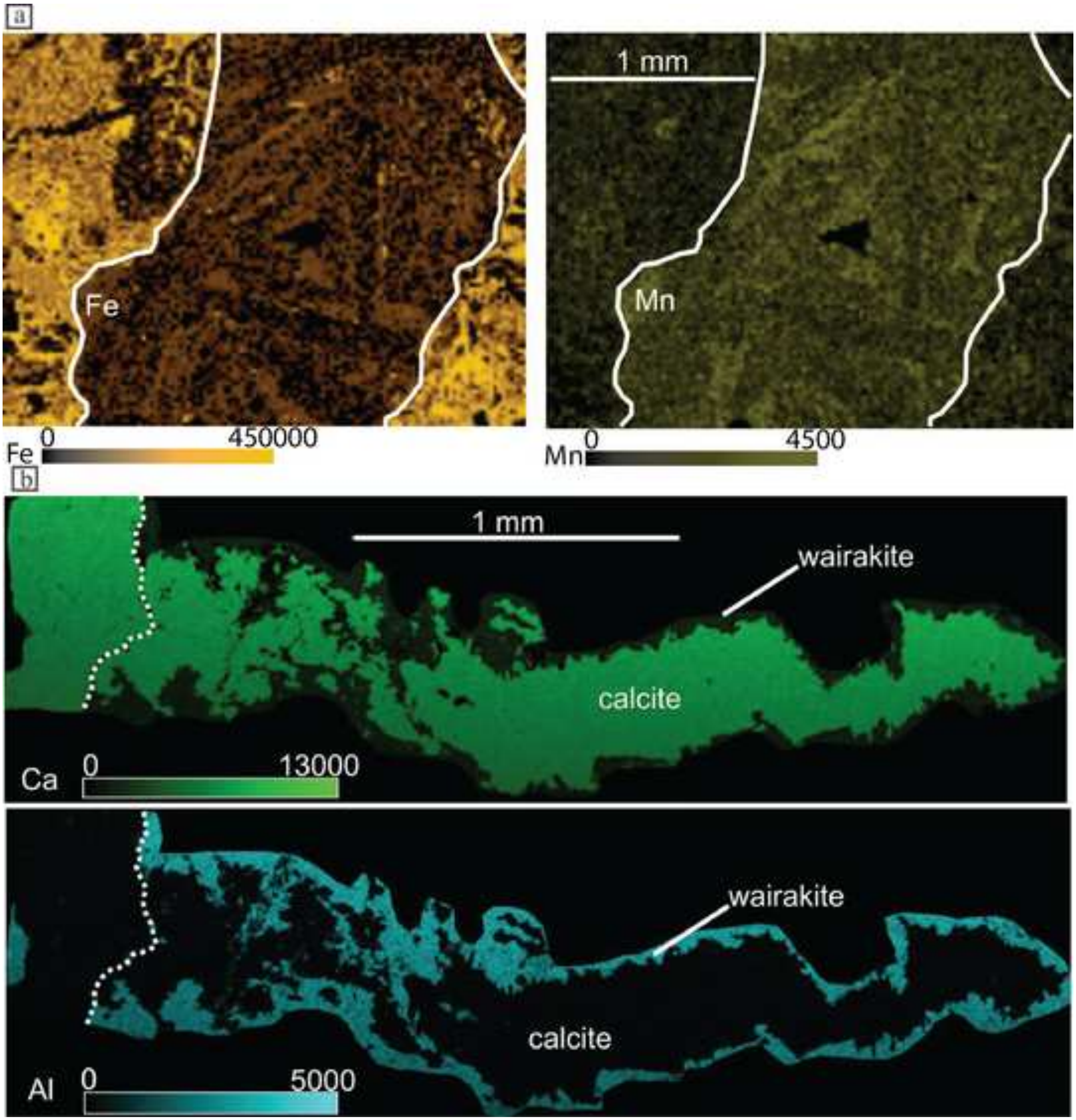

Figure

Click here to download high resolution image

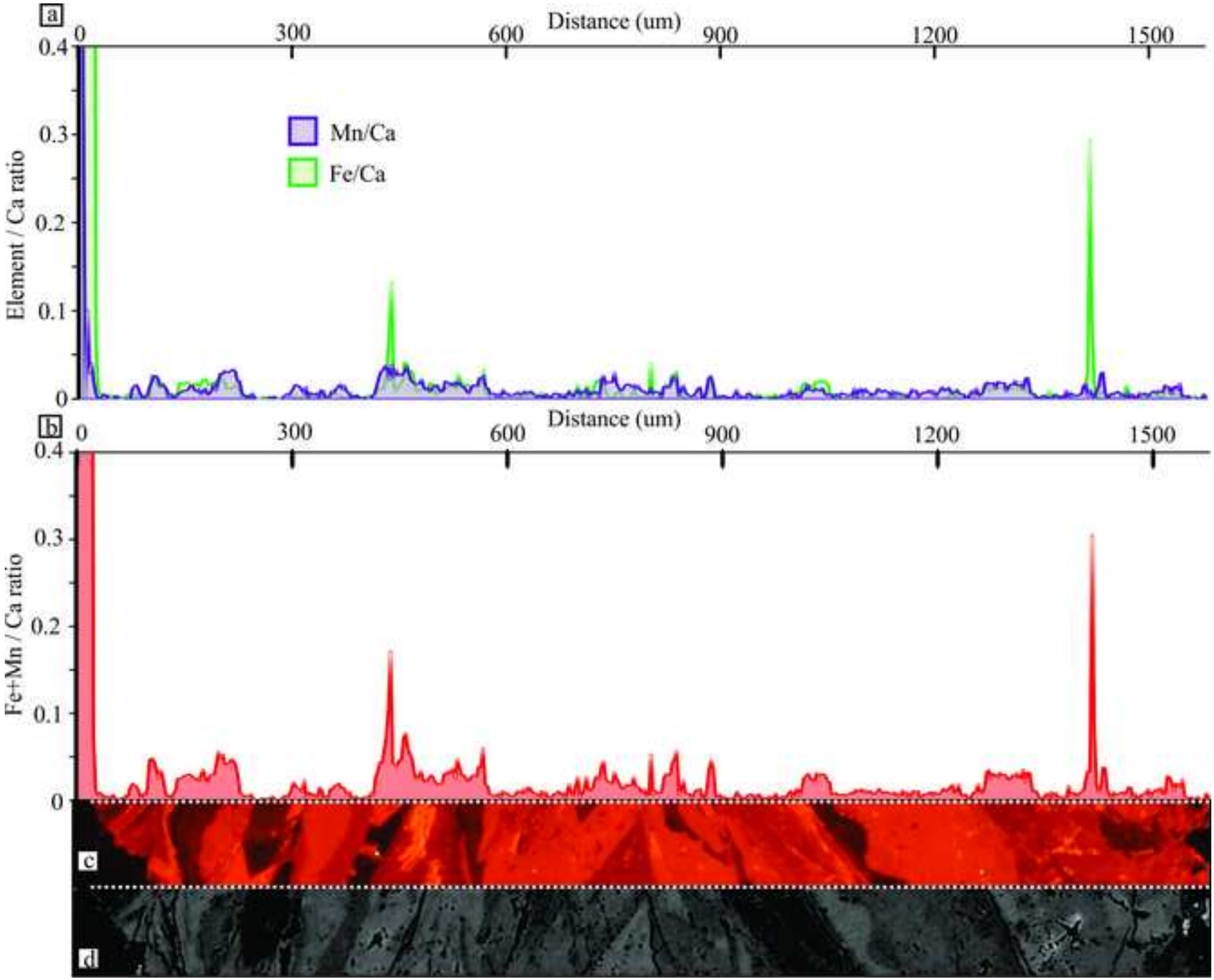

Figure

Click here to download high resolution image

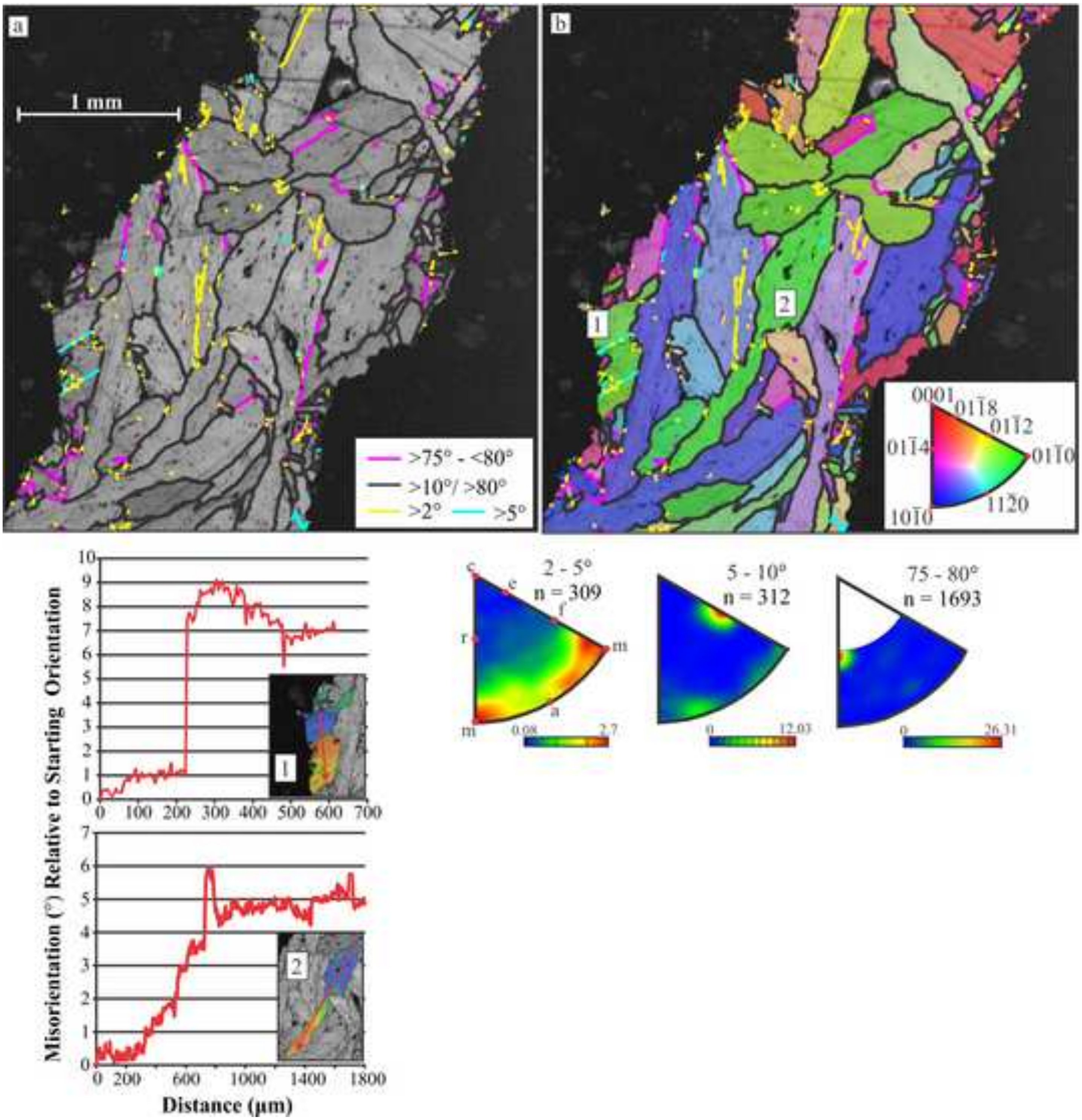

Figure
Click here to download high resolution image

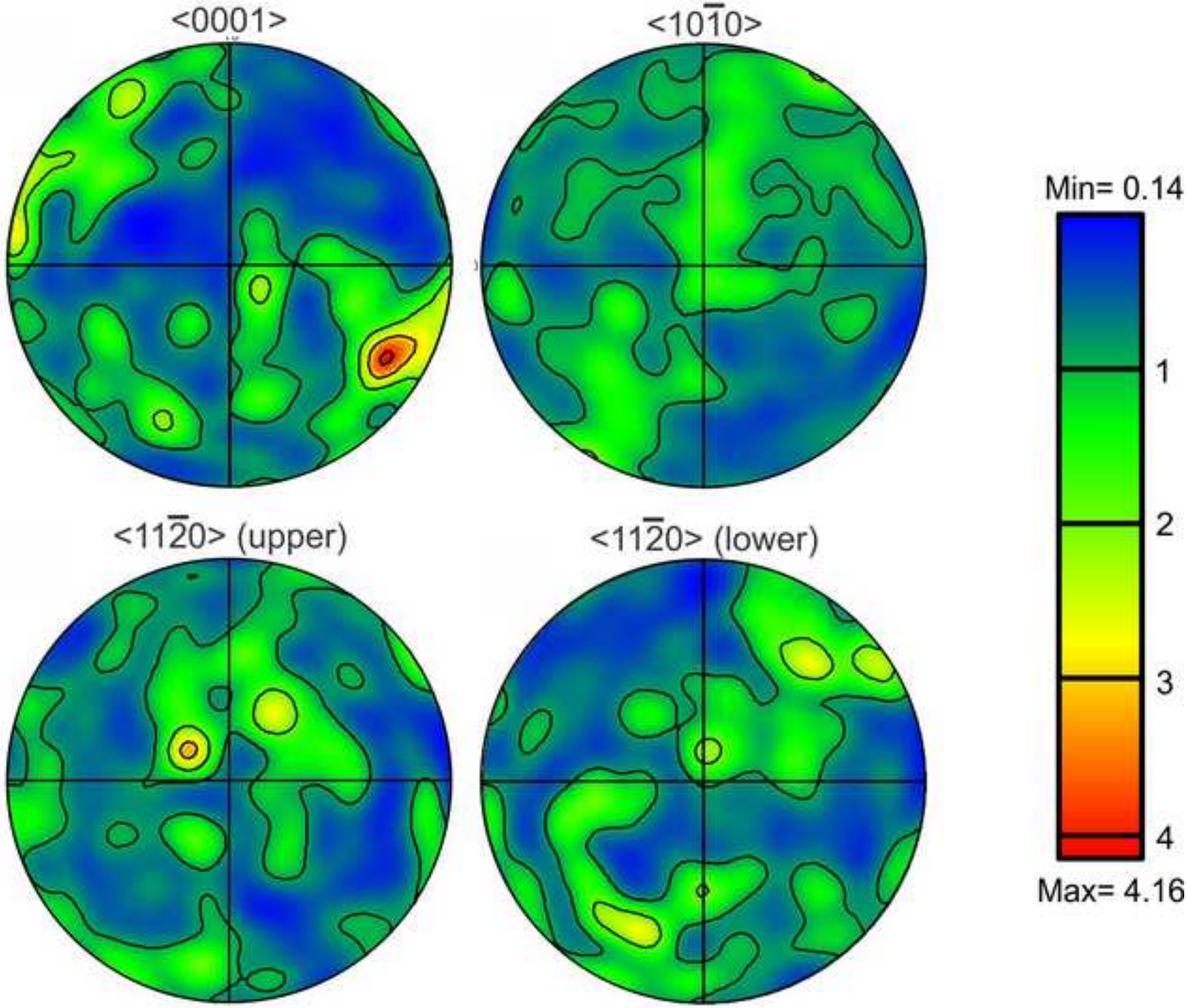

Figure
Click here to download high resolution image

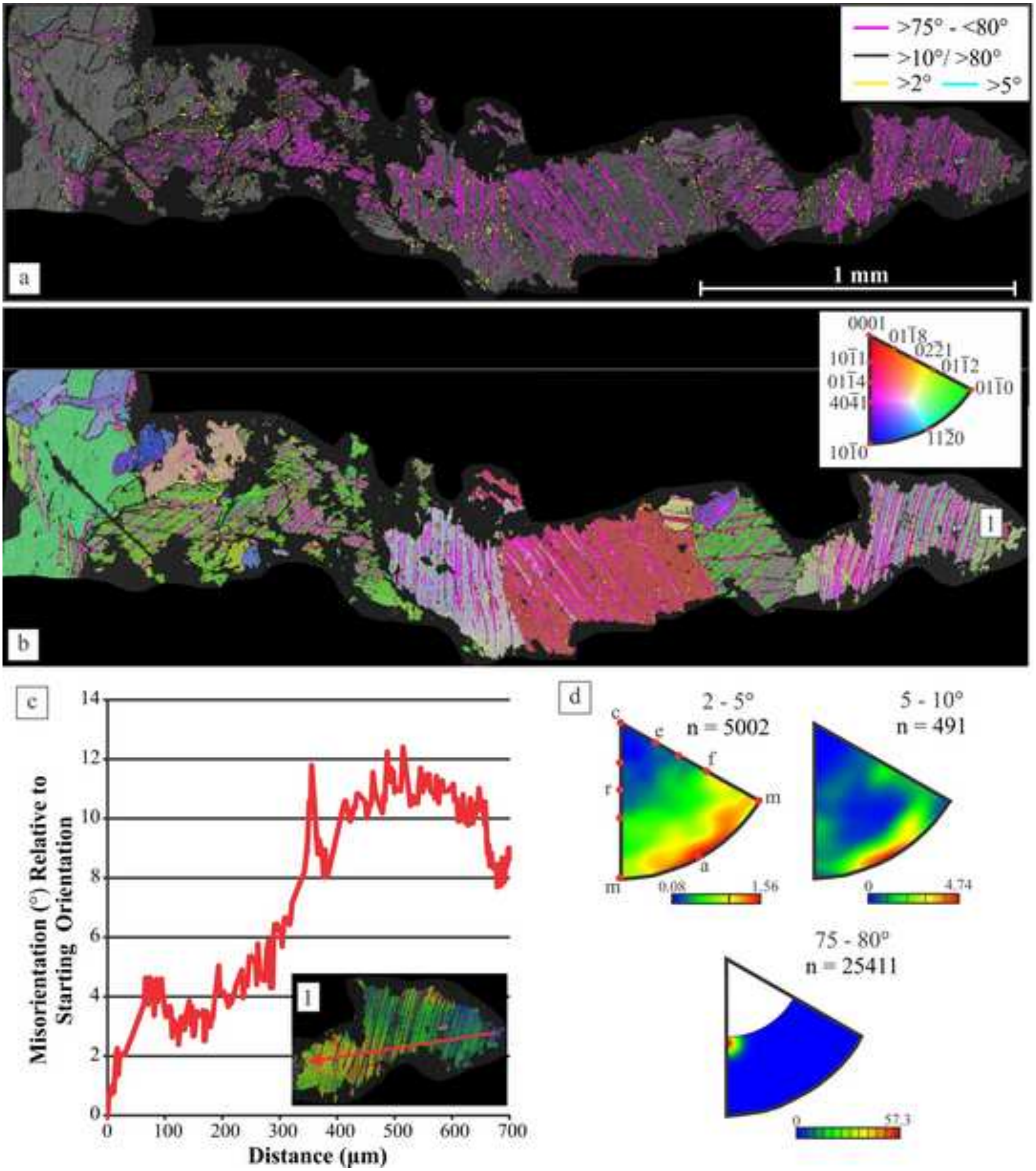

Figure

Click here to download high resolution image

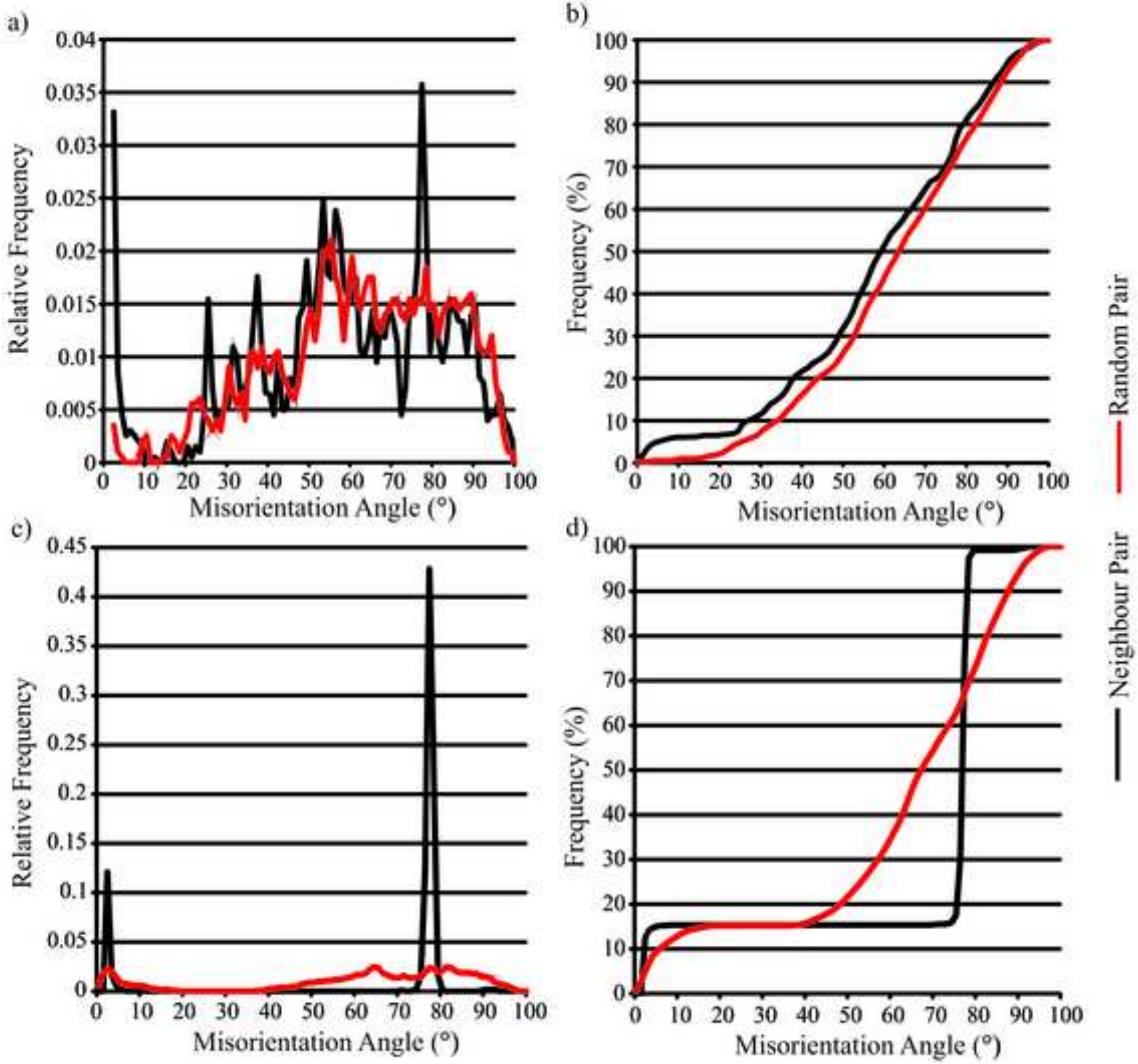

Figure

Click here to download high resolution image

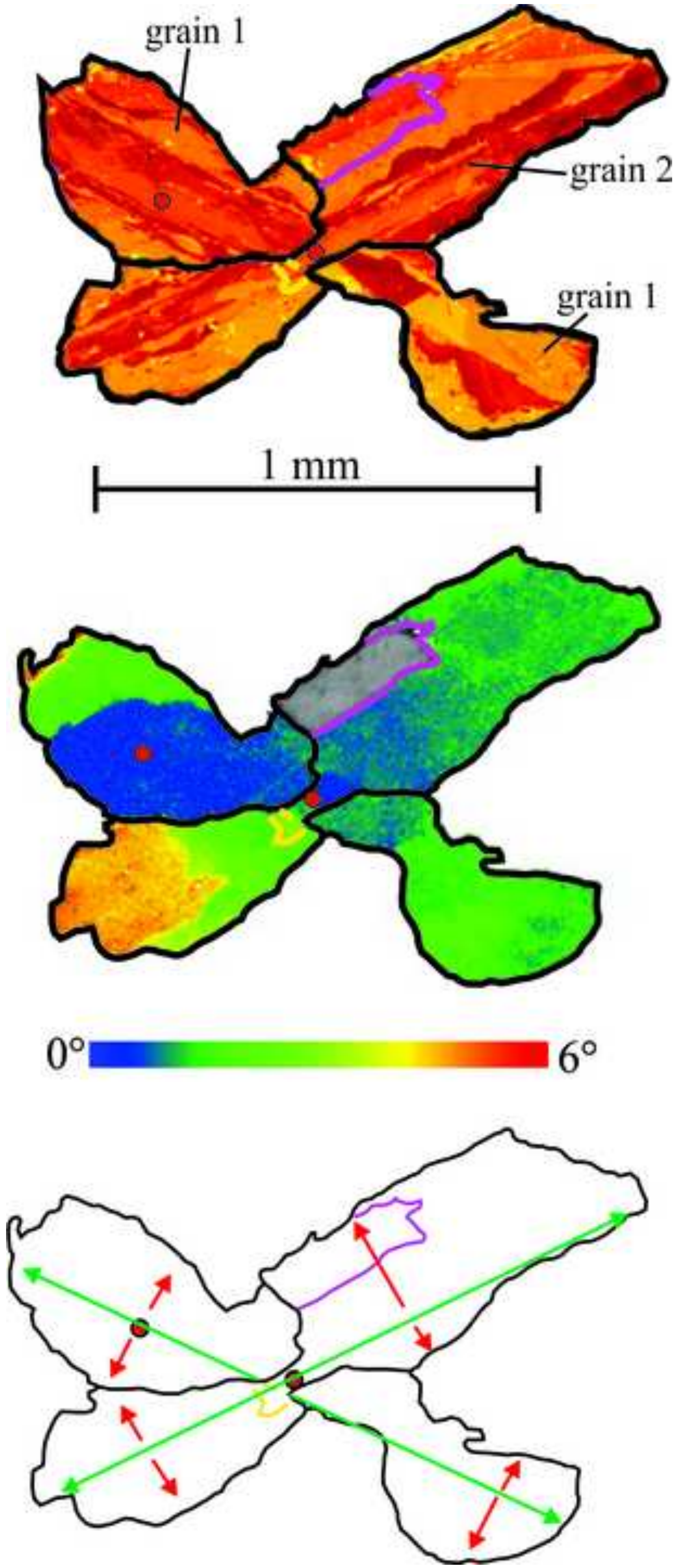

Figure
Click here to download high resolution image

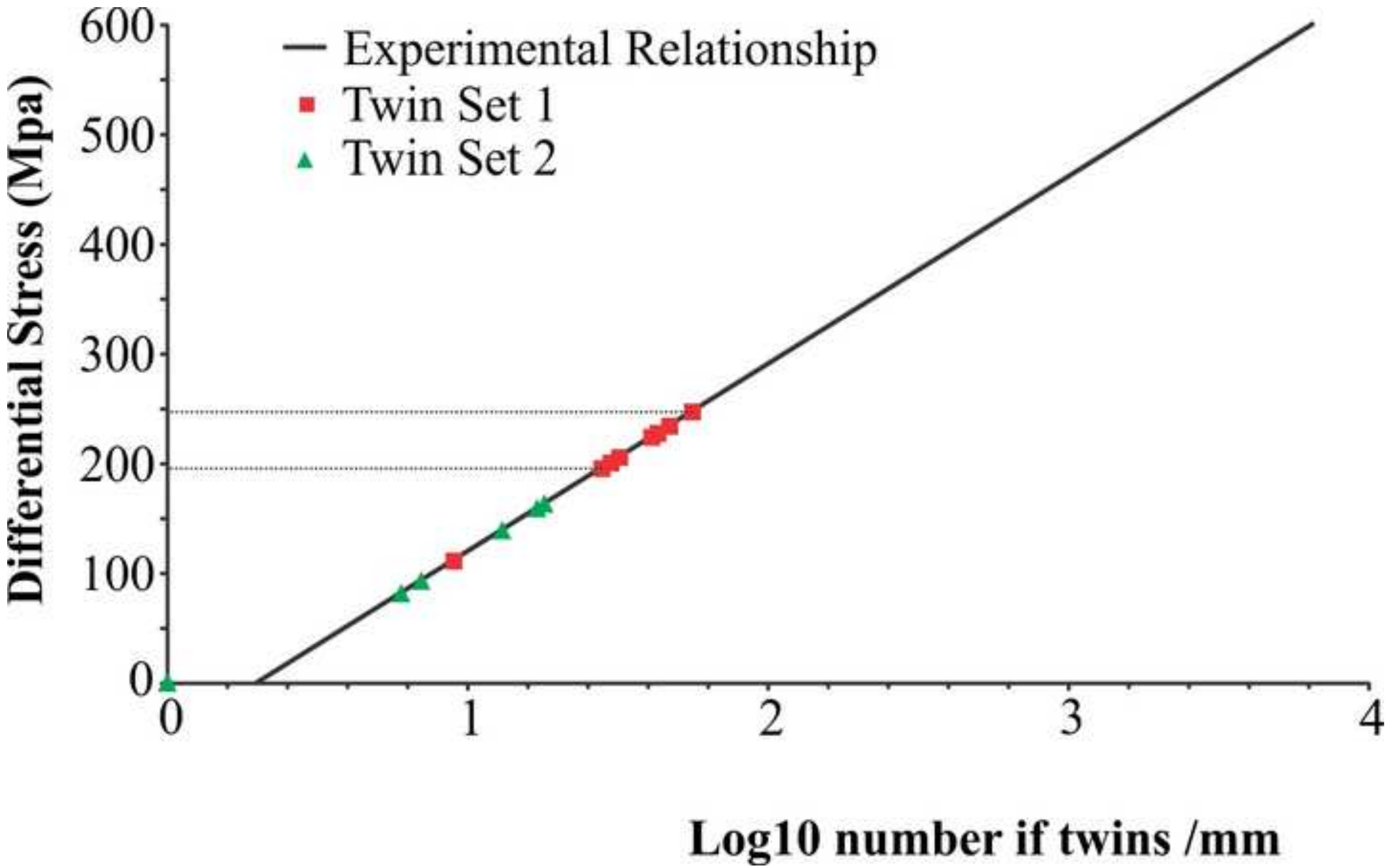

Figure
Click here to download high resolution image